Molecular Therapy
Nucleic Acids
Original Article

Developing antisense oligonucleotides for a *TECPR2* mutation-induced, ultra-rare neurological disorder using patient-derived cellular models

Luis A. Williams,[1,10] David J. Gerber,[1,10] Amy Elder,[1,10] Wei Chou Tseng,[1,10] Valeriya Baru,[1] Nathaniel Delaney-Busch,[1] Christina Ambrosi,[1] Gauri Mahimkar,[1] Vaibhav Joshi,[1] Himali Shah,[1] Karthiayani Harikrishnan,[1] Hansini Upadhyay,[1] Sakthi H. Rajendran,[1] Aishwarya Dhandapani,[1] Joshua Meier,[1] Steven J. Ryan,[1] Caitlin Lewarch,[1] Lauren Black,[2] Julie Douville,[2] Stefania Cinquino,[2] Helen Legakis,[2] Karsten Nalbach,[3] Christian Behrends,[3] Ai Sato,[4] Lorenzo Galluzzi,[4] Timothy W. Yu,[5] Duncan Brown,[1] Sudhir Agrawal,[6,7] David Margulies,[1] Alan Kopin,[8,9] and Graham T. Dempsey[1]

[1]Q-State Biosciences, 179 Sidney Street, Cambridge, MA 02139, USA; [2]Charles River Laboratories, Montreal, QC, Canada; [3]Munich Cluster for Systems Neurology, Ludwig-Maximilians-Universität München, Germany; [4]Department of Radiation Oncology, Weill Cornell Medical College, New York, NY, USA; [5]Boston Children's Hospital, 300 Longwood Avenue, Boston, MA 02115, USA; [6]University of Massachusetts Medical School, Department of Medicine, Worcester, MA 01655, USA; [7]Arnay Sciences LLC, Shrewsbury, MA 01545, USA; [8]Tufts University School of Medicine, Boston, MA, USA; [9]Luke Heller TECPR2 Foundation, Swampscott, MA, USA

Mutations in the *TECPR2* gene are the cause of an ultra-rare neurological disorder characterized by intellectual disability, impaired speech, motor delay, and hypotonia evolving to spasticity, central sleep apnea, and premature death (SPG49 or HSAN9; OMIM: 615031). Little is known about the biological function of TECPR2, and there are currently no available disease-modifying therapies for this disease. Here we describe implementation of an antisense oligonucleotide (ASO) exon-skipping strategy targeting *TECPR2* c.1319delT (p.Leu440Argfs*19), a pathogenic variant that results in a premature stop codon within *TECPR2* exon 8. We used patient-derived fibroblasts and induced pluripotent stem cell (iPSC)-derived neurons homozygous for the p.Leu440Argfs*19 mutation to model the disease *in vitro*. Both patient-derived fibroblasts and neurons showed lack of TECPR2 protein expression. We designed and screened ASOs targeting sequences across the *TECPR2* exon 8 region to identify molecules that induce exon 8 skipping and thereby remove the premature stop signal. *TECPR2* exon 8 skipping restored in-frame expression of a TECPR2 protein variant (TECPR2ΔEx8) containing 1,300 of 1,411 amino acids. Optimization of ASO sequences generated a lead candidate (ASO-005-02) with ~27 nM potency in patient-derived fibroblasts. To examine potential functional rescue induced by ASO-005-02, we used iPSC-derived neurons to analyze the neuronal localization of TECPR2ΔEx8 and showed that this form of TECPR2 retains the distinct, punctate neuronal expression pattern of full-length TECPR2. Finally, ASO-005-02 had an acceptable tolerability profile *in vivo* following a single 20-mg intrathecal dose in cynomolgus monkeys, showing some transient non-adverse behavioral effects with no correlating histopathology. Broad distribution of ASO-005-02 and induction of *TECPR2* exon 8 skipping was detected in multiple central nervous system (CNS) tissues, supporting the potential utility of this therapeutic strategy for a subset of patients suffering from this rare disease.

INTRODUCTION

Homozygous loss-of-function mutations in the *TECPR2* gene, encoding tectonin beta-propeller repeat-containing protein 2, cause an ultra-rare, monogenic neurological disorder characterized by intellectual disability, impaired speech, hypotonia, spasticity and severe motor delay, gastroesophageal reflux, areflexia, central sleep apnea, and premature death.[1,2] A homozygous pathogenic *TECPR2* single-base-pair deletion mutation, c.3416delT; p.Leu1139Argfs*75, was originally identified in five patients from three families of Bukharian Jewish origin.[1] The *TECPR2* mutation-induced disease was designated as an autosomal recessive form of complicated hereditary spastic paraparesis, spastic paraplegia 49 (SPG49), now classified as hereditary sensory and autonomic neuropathy type IX (HSAN9).

A second report identified two additional *TECPR2* mutations (c.1319delT; p.Leu440Argfs19 and c.C566T; p.Thr189Ile) among

Received 15 November 2021; accepted 17 June 2022;
https://doi.org/10.1016/j.omtn.2022.06.015.

[10]These authors contributed equally

Correspondence: Alan Kopin, Tufts University School of Medicine, Boston, MA, USA.
E-mail: akopin55@gmail.com
Correspondence: Graham T. Dempsey, Q-State Biosciences, 179 Sidney Street, Cambridge, MA 02139, USA.
E-mail: graham.dempsey@qstatebio.com

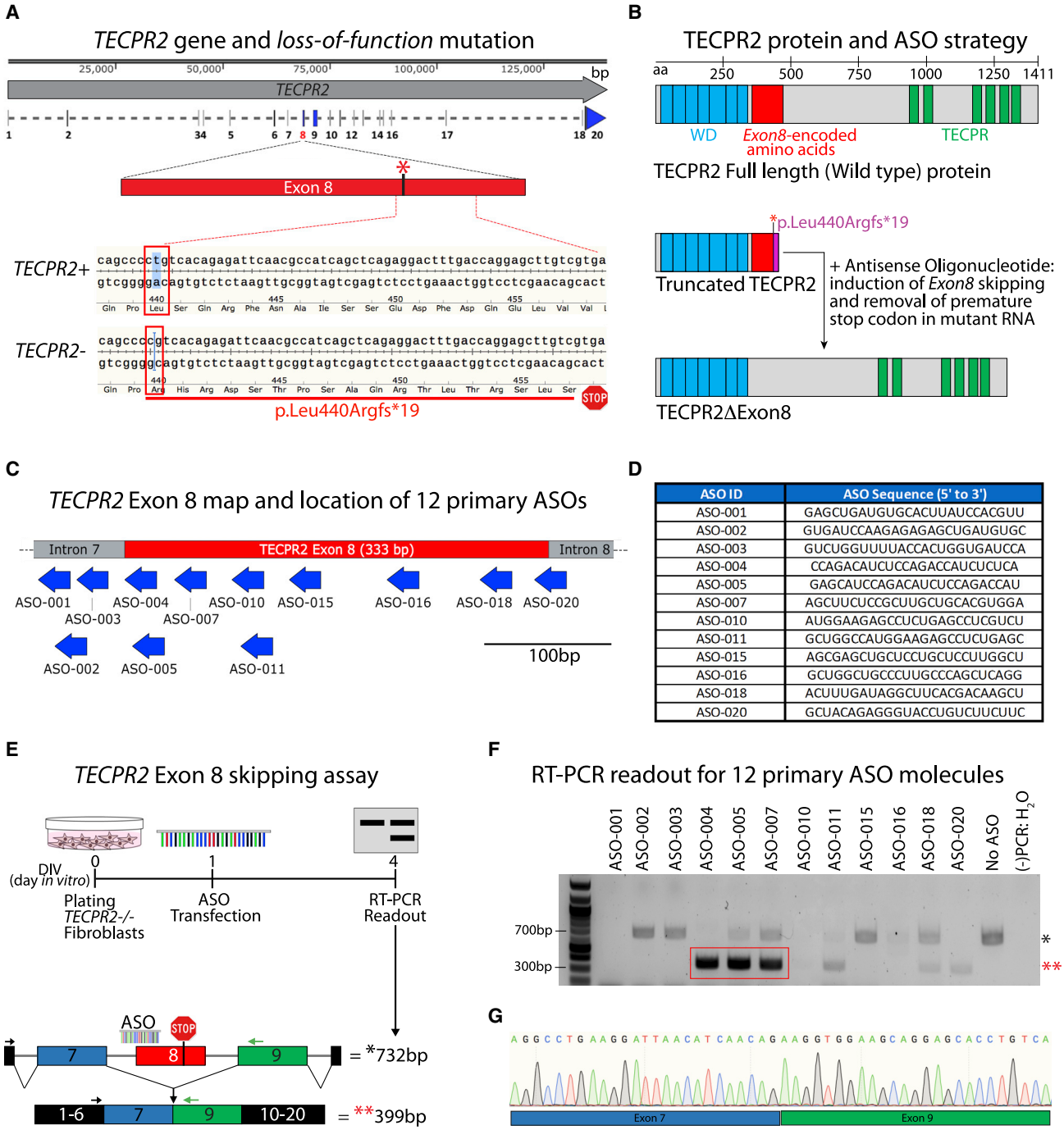

ASO ID	ASO Sequence (5' to 3')
ASO-001	GAGCUGAUGUGCACUUAUCCACGUU
ASO-002	GUGAUCCAAGAGAGAGCUGAUGUGC
ASO-003	GUCUGGUUUUACCACUGGUGAUCCA
ASO-004	CCAGACAUCUCCAGACCAUCUCUCA
ASO-005	GAGCAUCCAGACAUCUCCAGACCAU
ASO-007	AGCUUCUCCGCUUGCUGCACGUGGA
ASO-010	AUGGAAGAGCCUCUGAGCCUCGUCU
ASO-011	GCUGGCCAUGGAAGAGCCUCUGAGC
ASO-015	AGCGAGCUGCUCCUGCUCCUUGGCU
ASO-016	GCUGGCUGCCCUUGCCCAGCUCAGG
ASO-018	ACUUUGAUAGGCUUCACGACAAGCU
ASO-020	GCUACAGAGGGUACCUGUCUUCUUC

Figure 1. *TECPR2* gene and identification of ASO sequences inducing *TECPR2* exon 8 skipping

(A) Map of *TECPR2* gene showing exon/intron regions and highlighting exon 8 wild-type *TECPR2*+ and mutant *TECPR2*- (c.1319delT, p.Leu440Argfs*19) alleles. The SPG49 patient is homozygous for the mutation (*TECPR2*-/-). (B) Diagram of TECPR2 protein, highlighting annotated WD domain (predicted for residues 23–343) and TECPR repeat domain (predicted for residues 945–1353), along with the protein region (in red) encoded by *TECPR2* exon 8, which corresponds to 333 bp (111 amino acids). The premature stop codon in the SPG49 patient presumably results in truncated protein. ASO-mediated induction of *TECPR2* exon 8 skipping could restore expression of a shorter form of TECPR2 protein lacking exon 8-encoded sequence (TECPR2ΔExon8). (C) Diagram of *TECPR2* exon 8 and surrounding intron 7 and 8 regions showing location of initial set of 12 ASOs designed to induce exon 8 skipping. (D) Table listing ASO ID and sequence of initial set of 25-mer (25 nucleotides in length) ASOs used in primary screening. For these ASOs, all bases had 2′-O-methyl modification and all linkages were phosphorothioate chemistry. (E) Experimental outline for *TECPR2* exon 8 skipping assay using *TECPR2*-/- patient-derived fibroblasts. Enrichment of a shorter (minus 333 bp) PCR amplicon of ~399 bp is expected if *TECPR2* exon 8 skipping is induced. (F) DNA gel

(legend continued on next page)

three unrelated patients of non-Bukharian origin.[2] Two of these patients were of Ashkenazi Jewish origin and had compound heterozygous c.1319delT/c.C566T and homozygous c.1319delT/c.1319delT *TECPR2* genotypes, respectively. The third patient was of mixed Ashkenazi/Tunisian-Yamani/Kurdish origin and had the originally identified *TECPR2* mutation and the c.1319delT mutation in compound heterozygous state, c.1319delT/c.3416delT. The c.1319delT; p.Leu440Argfs19 frameshift mutation in exon 8 of *TECPR2* creates a premature termination codon and has estimated allele frequency of 0.003 in the Ashkenazi Jewish population,[2] with substantially lower global frequency. The most perilous feature of SPG49/HSAN9 is progressive, life-threatening respiratory dysregulation reported to have complex multisystem pathophysiology.[3]

The human *TECPR2* gene has 20 exons and encodes a full-length protein of 1,411 amino acids. There are two main structural annotations for TECPR2 in UniProt, an amino-terminal WD repeat domain with seven WD40 repeat motifs and a carboxy terminal TECPR domain containing six TECPR (tectonin beta-propeller repeat) motifs (Figure 1B). An LC3-interacting region has also been identified at the carboxy terminus of the protein.[4] These three domains exhibit strong conservation even for TECPR2 orthologs found in distant species, suggesting important roles in TECPR2 function.[4] The central region of the TECPR2 protein has no structural annotation. TECPR2 protein function is not well understood. TECPR2 has been proposed to act as a scaffold protein interacting with multiple partners.[4,5] Decreased markers of autophagy were observed in SPG49 patient-derived fibroblasts, suggesting a role for TECPR2 in autophagy.[1] A subsequent study, based on the TECPR2 protein interactome and functional analyses in human cell lines, reported a role of TECPR2 in endoplasmic reticulum (ER) export and autophagosome formation.[4] Recently, impaired basal autophagic flux with accumulation of autophagosomes was observed in SPG49 patient fibroblasts, indicating a potential role for TECPR2 in targeting of autophagosomes to lysosomes.[6] Expression of full-length TECPR2 or its TECPR domain was found to rescue aspects of the autophagy impairment, suggesting that the TECPR domain may be sufficient for regulating basal autophagy in fibroblasts.[6]

Two studies have characterized the effects of *TECPR2* mutations in the central nervous system (CNS) *in vivo*. A spontaneous missense mutation (c.4009C>T or p.R1337W) affecting a highly conserved region in *TECPR2* was identified in Spanish water dogs as the cause of an autosomal recessive neuroaxonal dystrophy marked by accumulation of spheroids resembling autophagosomes in the gray matter of the cerebral hemispheres, the cerebellum, the brain stem, and the spinal cord sensory pathways.[7] Recently, *Tecpr2* knockout mice were shown to exhibit neuroaxonal dystrophy with accumulation of autophagosomes in medulla oblongata of brain stem and dorsal tracts of spinal cord.[8] These studies link *TECPR2* mutation with perturbed autophagy and neurodegeneration *in vivo*. Despite these insights, neuronal disease mechanisms and the pathogenic basis of respiratory insufficiency in SPG49 remain poorly understood, and since TECPR2 is not a traditional drug target for small molecule modulation, therapeutic avenues for SPG49 are challenging.

Recently, antisense oligonucleotides (ASOs) that induce exon skipping have emerged as a direct therapeutic approach to address pathogenic frameshift and nonsense mutations.[9,10] The clinical promise of this approach was reflected by the approval of Eteplirsen, an exon-skipping agent for Duchenne muscular dystrophy (DMD).[9,11] The approval of nusinersen, a splice switching ASO for spinal muscular atrophy administered by intrathecal injection, has also validated this ASO therapeutic modality for CNS disorders.[9,12–14]

In its simplest form, splice-modulating ASO strategies can be used to target pathogenic genetic variants in exons that are dispensable and can be removed by in-frame skipping of exonic sequence. As *TECPR2* exon 8 encodes a non-structured region of the protein and is 333 nucleotides in length, an ASO-mediated exon 8-skipping approach is a potentially feasible therapeutic approach for individuals with *TECPR2* exon 8 mutations. The p.Leu440Argfs19 mutation is primarily present in individuals of Ashkenazi Jewish origin, with allele frequency estimated at 0.003 in that population.[2] The exon 8-skipping strategy may be most effective for patients homozygous for this mutation that have two relevant target alleles. However, the strategy could benefit patients with the exon 8 mutation in compound heterozygous context since it could provide functional rescue from the single relevant target allele. It is important to note that other pathogenic *TECPR2* mutations, including two additional exon 8 frameshift mutations reported in ClinVar, appear to be very rare. The patient population eligible for this specific therapeutic approach is thus expected to predominantly include individuals having the p.Leu440Argfs19 exon 8 mutation. Based on estimated carrier frequencies of exon 8 and other pathogenic *TECPR2* alleles,[15] and the shortened lifespan reported for SPG49 patients, this specific eligible patient population is expected to be up to a few hundred patients worldwide.

Here, we report the identification and optimization of *TECPR2* exon 8-skipping ASOs. We show that a lead ASO rescues TECPR2 protein expression in dermal fibroblasts and induced pluripotent stem cell (iPSC)-derived neurons from an SPG49 patient. The rescued form of TECPR2 protein lacking exon 8 (TECPR2ΔEx8) exhibits the distinct, punctate neuronal distribution pattern of full-length TECPR2, providing a surrogate measure of its functionality. The candidate ASO induced *TECPR2* exon 8 skipping throughout the CNS and had an acceptable tolerability profile in cynomolgus

inverse image with results of initial screening of 12 primary ASOs showing that treatment of *TECPR2*-/- patient fibroblasts with ASO-004, ASO-005, and ASO-007 can lead to significant enrichment of ~399-bp PCR amplicon (highlighted in red rectangle and with red asterisks [**]), corresponding to *TECPR2* transcript minus exon 8. (–)PCR:H_2O, water was used as negative control for PCR assay. (G) Sanger sequencing chromatogram of purified lower PCR amplicon (~399 bp) obtained from samples treated with ASO-005, demonstrating *TECPR2* exon 8 skipping with precise splicing of exon 7 and exon 9 sequences.

monkeys following a single intrathecal dose. Pending full safety evaluation, these results support the exon 8-skipping ASO as a promising therapeutic strategy for SPG49 patients with *TECPR2* exon 8 mutation.

RESULTS

Identification and optimization of ASO sequences inducing *TECPR2* exon 8 skipping

A schematic of the *TECPR2* gene and location of the exon 8 pathogenic c.1319delT (p.Leu440Argfs*19) mutation is shown in Figure 1A. The human *TECPR2* gene contains 20 exons and encodes a full-length protein of 1,411 amino acids. The mutation results in a frameshift and premature termination codon within exon 8. Since *TECPR2* exon 8 is 333 nucleotides in length, ASO-mediated exon 8 skipping would preserve the *TECPR2* reading frame and generate an mRNA transcript encoding a 1,300-amino acid form of TECPR2 protein (TECPR2ΔEx8) missing 111 amino acid (362–472) residues (Figure 1B). Importantly, TECPR2ΔEx8 retains the WD40 and TECPR repeat domains and lacks only a small portion of the central unstructured region, compatible with the concept that TECPR2ΔEx8 protein may retain wild-type function.

To identify candidate ASO sequences for exon 8 skipping, 12 25-mer ASOs spanning the *TECPR2* exon 8 pre-mRNA region were designed, synthesized as 2′-O-methyl phosphorothioates, and selected for screening (Figures 1C and 1D). To test for exon 8-skipping activity, dermal fibroblasts derived from an SPG49 patient homozygous for the exon 8 *TECPR2* mutation (*TECPR2-/-*) were transfected separately with each of the 12 ASOs at 1 μM and analyzed using an RT-PCR assay to detect the full-length (732 bp) and the exon 8-skipped (399 bp) *TECPR2* mRNA amplicons (Figure 1E). After ASO treatment of the patient fibroblasts for 72 h, three ASOs, ASO-004, ASO-005, and ASO-007, yielded a clear PCR band of ∼399 bp, indicating potential exon 8-skipping activity (Figure 1F). Sequencing of the lower PCR product confirmed precise *TECPR2* exon 8 skipping (Figure 1G). Subsequent analyses with optimized conditions (reduced ASO concentration, 300 nM versus 1 μM, and increased incubation time, 120 h versus 72 h) identified at least two additional ASOs, ASO-018 and ASO-020, targeting the 3′ end of exon 8 (Figure 1C) that induce robust exon 8 skipping (Figure S1).

The three most active ASOs (ASO-004, ASO-005, and ASO-007) target the first 64 nucleotides of *TECPR2* exon 8 and define an active target region for exon 8 skipping (Figure 2A). We sought to identify an ASO lead molecule targeting this region with optimal features for therapeutic application, including shorter length, potency in the nanomolar range, clinically validated chemistry, and target sequence conservation to enable preclinical *in vivo* studies. The active target region was analyzed for sequence homology to animal species relevant for preclinical studies. The first 37 bases of the region and the last three bases of intron 7 have sequence identity with cynomolgus monkey (Figure 2A), and significantly lower sequence similarity to homologous regions in mouse and rat *Tecpr2*. To identify optimal ASO lead molecules with target sequence conservation in cynomolgus monkey, given its importance as a preclinical toxicology species, micro-tiling of the 40-base region was performed using sets of 18-mer and 21-mer ASOs, for a total of 41 ASO sequences (Figures S1 and S2) as well as shorter active derivatives of ASO-004 and ASO-005 (Figures S1 and S2). *TECPR2-/-* patient fibroblasts were transfected separately with the micro-tiling ASOs at 1 μM and analyzed using the patient fibroblast RT-PCR assay (Figure 1E). Multiple active ASOs yielding the 399-bp PCR product were identified (Figure 2B). Further prioritization of active ASOs was carried out based on bioinformatic analysis to eliminate those with potential off-target homologies. The initial ASO screening was performed using ASO chemistry with all RNA bases with 2′-O-methyl sugar modifications and all phosphorothioate linkages, based on efficiency and cost considerations. To assess selected ASOs using the clinically validated ASO chemistry to be applied in our clinical candidate, a set of nine prioritized leads among all ASOs were selected for conversion to chemistry with all RNA bases with 2′-*O*-methoxyethyl (2′-MOE) sugar modifications, 5-methyl cytosine and 5-methyl uracil bases, and all phosphorothioate linkages, the same chemistry employed in Spinraza (nusinersen).[16] These nine ASOs share a core 13-base sequence (Figure 2C) and were tested in six-point concentration-response (300–1 nM, ∼3-fold dilutions) in the *TECPR2-/-* patient fibroblast RT-PCR assay (Figure 2D). Side-by-side comparisons of ASO chemistries demonstrated that the transition from 2′-O-methyl to 2′-MOE RNA bases did not change the ASO-mediated exon 8-skipping activity (Figure S3). ASO-005-02 (a 21-mer derivative of ASO-005) was the most potent ASO lead with a half maximal effective concentration (EC_{50}) of ∼27.3 nM (Figure 2E). Two additional ASO sequences (ASO-059 and ASO-066, the latter being a 19-mer derivative of ASO-005) were also selected as back-up ASO leads based on robust RT-PCR assay results. ASO-005-02 was selected for further characterization in patient-derived cellular models.

Rescue of TECPR2 protein expression in *TECPR2-/-* patient fibroblasts and iPSC-derived neurons

TECPR2-/- patient fibroblasts do not express TECPR2 protein as assessed by immunocytochemistry when compared with fibroblasts obtained from healthy relatives of the SPG49 patient (Figure S4). The available antibody used for this analysis could detect overexpression of recombinant full-length TECPR2 and TECPR2 lacking exon 8-encoded sequence (TECPR2ΔEx8) in transfected cell lines by immunoblotting but was not effective with the same method at detecting endogenous TECPR2 in fibroblasts (Figure S5). Therefore, we utilized TECPR2 immunocytochemistry to assess ASO-mediated rescue of TECPR2 protein expression in patient-derived fibroblast cells. Transfection of patient fibroblasts with ASO-005-02 at 100 nM and 300 nM induced robust rescue of TECPR2 protein expression (Figures 3A–3C), indicating effective cellular expression of TECPR2 lacking exon 8-encoded sequence. Levels of protein expression in ASO-treated patient fibroblasts were similar to those detected in both *TECPR2+/+* and *TECPR2+/-* fibroblasts (Figure 3C), although it was noted that only minimal differences in protein detection were found between the *TECPR2+/+* and

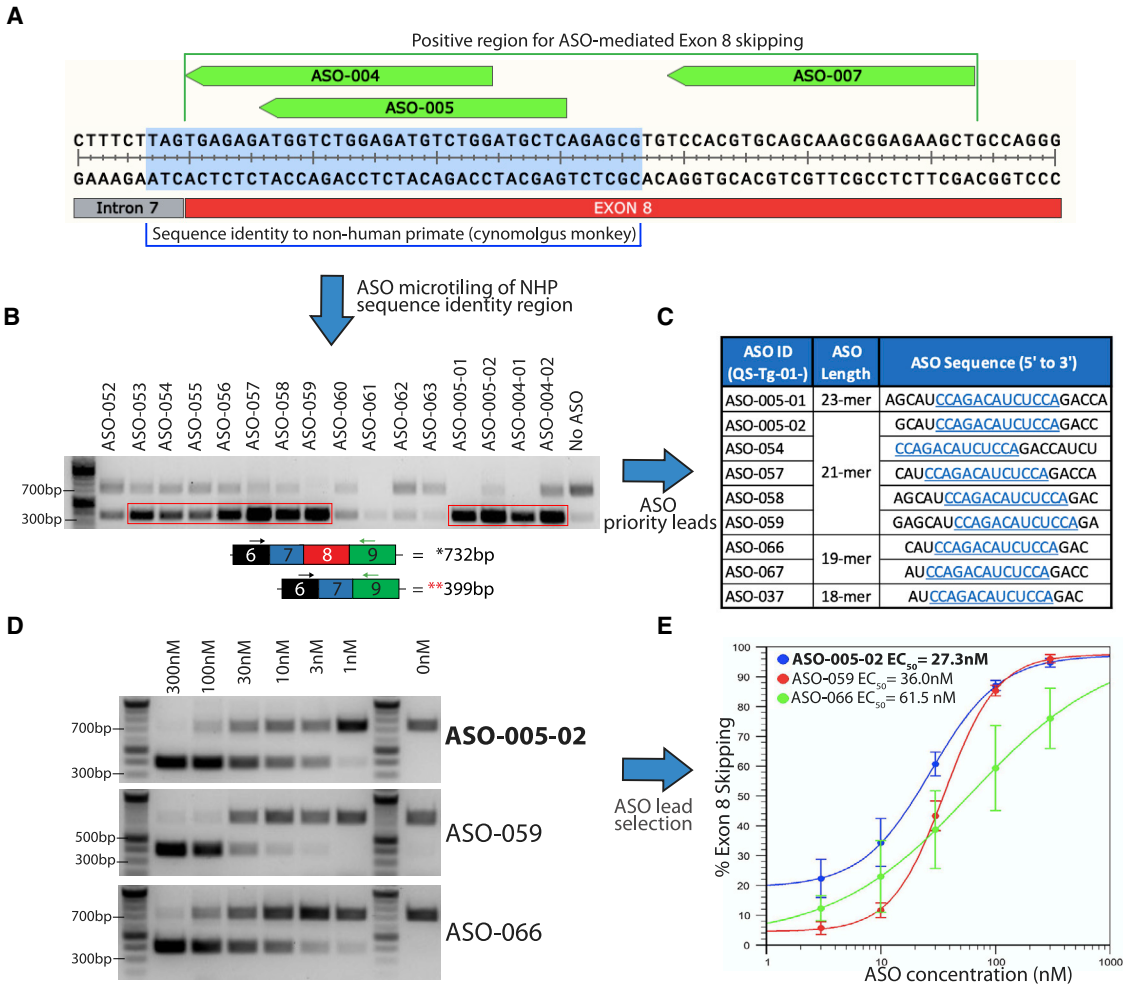

ASO ID (QS-Tg-01-)	ASO Length	ASO Sequence (5' to 3')
ASO-005-01	23-mer	AGCAUCCAGACAUCUCCAGACCA
ASO-005-02	21-mer	GCAUCCAGACAUCUCCAGACC
ASO-054		CCAGACAUCUCCAGACCAUCU
ASO-057		CAUCCAGACAUCUCCAGACCA
ASO-058		AGCAUCCAGACAUCUCCAGAC
ASO-059		GAGCAUCCAGACAUCUCCAGA
ASO-066	19-mer	CAUCCAGACAUCUCCAGAC
ASO-067		AUCCAGACAUCUCCAGACC
ASO-037	18-mer	AUCCAGACAUCUCCAGAC

Figure 2. ASO tiling, optimization, and selection of ASO leads that induce *TECPR2* exon 8 skipping

(A) *TECPR2* exon 8 region showing binding locations of the three most active exon 8-skipping ASOs (ASO-004, ASO-005, and ASO-007, shown in green). Sub-region with 100% sequence identity to cynomolgus monkey is highlighted in light blue. (B) DNA gel inverse image with a subset of PCR results of additional screening after ASO micro-tiling and trimming of initial active sequences. Enrichment of lower PCR amplicon (~399 bp) can be detected after treatment with several of these ASOs (highlighted in red rectangle). (C) Subset of nine ASO sequences of different length selected as priority leads. All sequences listed were then synthesized using 2′-*O*-methoxyethyl bases and 5-methyl cytosine and uracil bases, with phosphorothioate backbone. All ASO sequences share a core 13-base sequence highlighted in blue and underscored. (D) DNA gel inverse images of *TECPR2* exon 8-skipping PCR results for ASO leads ASO-005-02, ASO-059, and ASO-066, assayed at different concentrations (300–1 nM). (E) Half maximal effective concentration (EC_{50}) for ASO leads ASO-005-02, ASO-059, and ASO-066 calculated using percentage of *TECPR2* exon 8 skipping (estimated as fraction of lower PCR amplicon over total PCR product) at different concentrations (each data point corresponds to n = 3 independent rounds of ASO treatment, each with n = 1 RT-PCR assay). ASO-005-02 (in blue) was the most potent (EC_{50} = ~27.3 nM) and was selected for further studies in patient-derived cells.

TECPR2+/- fibroblast samples, perhaps due to limitations in the detection efficiency of the antibody in this assay. These data indicated that ASO-induced exon 8 skipping could induce protein expression of TECPR2ΔEx8 to levels of endogenous TECPR2 detected in healthy control samples.

Since SPG49 is primarily a neurological disorder,[1,2] we sought to confirm the activity of the lead ASO candidate in neurons. Neurons were differentiated from iPSC lines derived from the SPG49 patient and unaffected *TECPR2*+/+ and *TECPR2*+/- relatives. Neurons were produced using a transcriptional programming approach whereby the proneuronal transcription factor NGN2 was overexpressed in iPSCs (Figure 4A) to generate a homogenous population of cortical excitatory neurons (NGN2 neurons).[17,18] Differentiated neurons were treated at plating with ASO-005-02 at 5 μM, using gymnotic delivery. A scrambled, non-targeting ASO was used as a negative control. Immunocytochemistry analysis of *TECPR2*+/- NGN2 neurons treated with the scrambled control ASO indicated that all neurons identified by staining for MAP2 (microtubule-associated protein 2) were positive for TECPR2 staining (eight out of eight in field shown, Figures 4B and 4C). Patient-derived NGN2 neurons treated with control scrambled ASO were

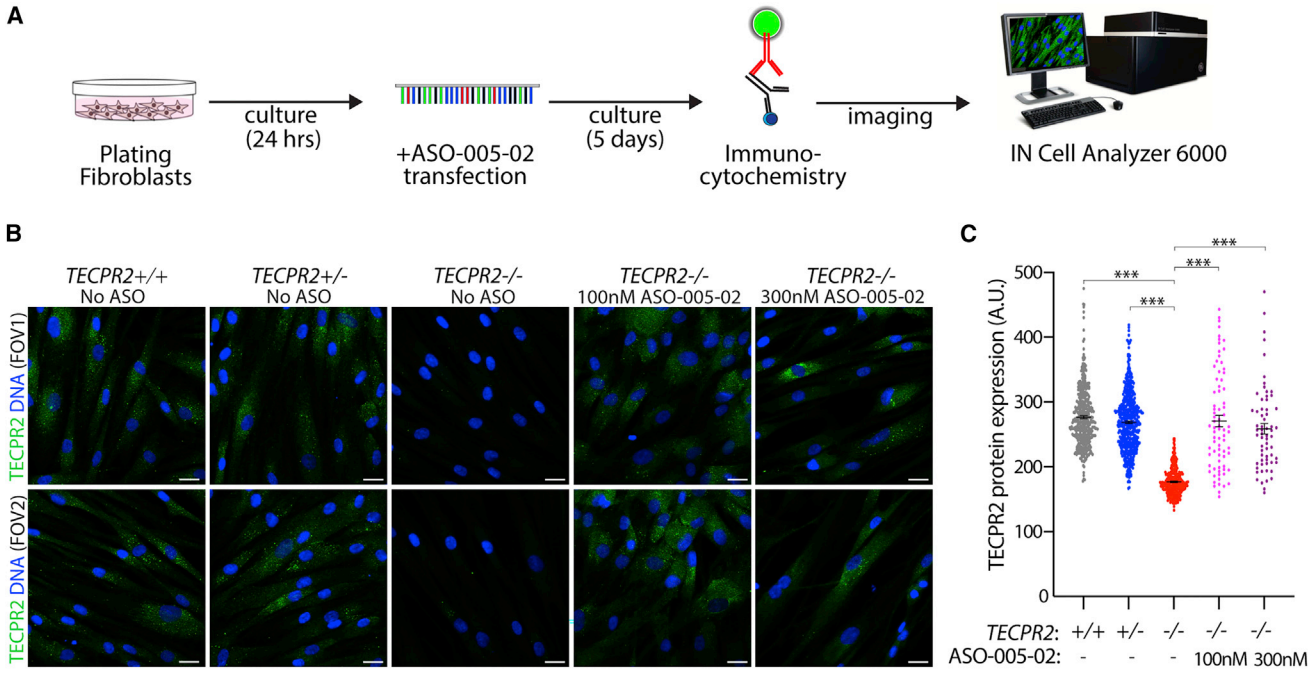

Figure 3. ASO-005-02 can rescue TECPR2 protein expression in *TECPR2*-/- (SPG49) patient-derived fibroblasts

(A) Experimental outline for rescue of TECPR2 protein expression assay, using immunocytochemistry with a rabbit polyclonal antibody raised against human TECPR2 as the primary antibody. TECPR2 immunoreactivity in *TECPR2*-/- fibroblasts was assessed 5 days after treatment with ASO-005-02 using an IN Cell Analyzer 6000 platform. (B) Representative immunofluorescence images obtained from two fields of view (FOVs) for each of the different *TECPR2* genotype and ASO treatment conditions, showing TECPR2 immunoreactivity with green signal and nuclear stain in blue. While untreated *TECPR2*-/- fibroblasts show no TECPR2 immunoreactivity, the same patient-derived cells treated with 100 nM or 300 nM lead ASO-005-02 show TECPR2 signal comparable with that of healthy control genotypes *TECPR2*+/+ and *TECPR2*+/- (scale bar, 20 μm). (C) Quantitative immunocytochemistry of the different *TECPR2* genotype and ASO conditions. Each data point represents a single cell for which TECPR2 fluorescence signal has been estimated (n = 60–400 cells per condition, 16–32 FOVs, error bars = SEM, ***p < 0.001 [pairwise t test FDR-corrected p value]).

negative for TECPR2 immunoreactivity, indicating lack of TECPR2 protein expression (none out of seven in field shown, Figures 4D and 4E). Treatment of patient-derived neurons with ASO-005-02 resulted in TECPR2 protein expression (TECPR2ΔEx8) in a percentage of cells (five out of 15 in field shown; Figures 4F and 4G). Quantification across multiple fields of view indicated that 100% of *TECPR2*+/+ and *TECPR2*+/- NGN2 neurons treated with scrambled control ASO were positive for TECPR2 protein expression, while a background of ~2.8% of patient-derived *TECPR2*-/- NGN2 neurons treated with scrambled control ASO showed some level of TECPR2 immunoreactivity (Figure 4H). Approximately 22.5% (15 out of 85) of patient-derived *TECPR2*-/- NGN2 neurons treated with ASO-005-2 showed clear TECPR2 immunoreactivity (Figures 4F–4H). Gymnotic delivery of ASOs to cell lines, including cultured human iPSC-derived neurons, is known to be inefficient, consistent with induction of measurable TECPR2 protein expression in only a fraction of the *TECPR2*-/- cells treated with ASO-005-02. Neuronal uptake of ASOs has been shown to be more efficient *in vivo*.[19–21]

TECPR2 and TECPR2ΔExon8 neuronal localization in patient iPSC-derived neurons

To examine the neuronal subcellular distribution of TECPR2 protein and TECPR2ΔEx8, high-resolution immunocytochemistry analysis was performed on iPSC-derived NGN2 neurons treated with ASOs by gymnotic delivery (5 μM) at plating and cultured for 45 days. Cells were co-stained for neuronal markers β-III TUBULIN (present in all neurites), MAP2 (present in soma and proximal dendrites), and for TECPR2. As shown in Figure 5A–5D′, scrambled control ASO-treated *TECPR2*+/+ NGN2 neurons exhibited a distinct, subcellular TECPR2 expression pattern with three discrete types of TECPR2-positive puncta: (1) broad, speckled puncta pattern within soma and proximal dendrites (Figure 5D, cyan arrowhead); (2) small discrete puncta in thick and thin β-III TUBULIN-positive neurites (Figure 5D, yellow arrowhead); and (3) rare large puncta in thin β-III TUBULIN-positive neurites (Figures 5D and 5D′, green arrowhead). *TECPR2*+/- iPSC-derived NGN2 neurons treated with scrambled control ASO showed a similar pattern of staining (Figures 5E–5H′). *TECPR2*-/- patient-derived NGN2 neurons treated with the scrambled control ASO showed no TECPR2 immunoreactivity and absence of the punctate expression pattern (Figures 5I–5L′). Three examples presented in Figures 5M–P′, 5Q–T′, and 5U–X′ show that treatment of patient *TECPR2*-/- NGN2 neurons with ASO-005-2 rescued all three types of neuronal TECPR2-positive puncta observed in *TECPR2*+/+ NGN2 neurons. The preserved punctate expression pattern is consistent with the functional integrity of TECPR2ΔEx8 and provides evidence that the TECPR2ΔEx8 protein is synthesized,

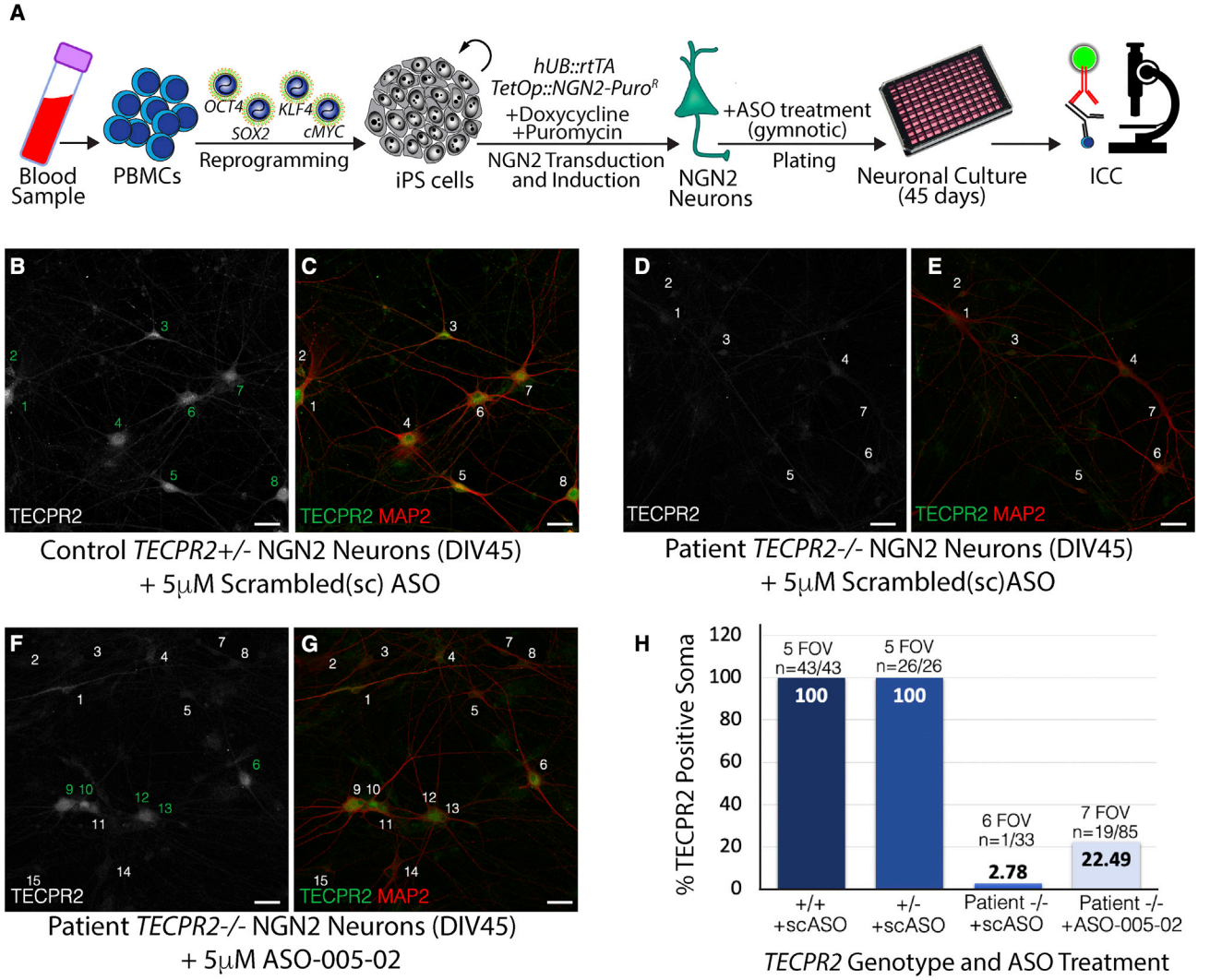

Figure 4. ASO-005-02 can rescue TECPR2 protein expression in *TECPR2*-/- (SPG49) patient iPSC-derived neurons

(A) Generation of SPG49 patient iPSC lines and cortical excitatory neurons via reprogramming of peripheral blood mononuclear cells (PBMCs) with pluripotency factors (OCT4, SOX2, KLF4, and cMYC) and transcriptional programming with pro-neuronal factor NEUROGENIN-2 (NGN2). *TECPR2-/-* patient and *TECPR2+/-* control iPSC-derived neurons were treated with either 5 μM ASO-005-02 or a scrambled (non-targeting) negative control ASO during plating (single treatment, gymnotic delivery) and cultured for 45 days to allow neuronal maturation. Effect of ASO treatment on TECPR2 expression was assessed using immunocytochemistry. (B and C) Control *TECPR2+/-;* NGN2 neurons show clear TECPR2 immunoreactivity in soma and neuronal processes. (B) TECPR2 signal only and (C) a merge of TECPR2 (in green) with the pan-neuronal marker MAP2 (in red). Individual neurons in these panels are indicated (numbers 1–8). (D and E) SPG49 patient *TECPR2-/-* NGN2 neurons treated with scrambled (negative control) ASO do not show clear TECPR2 immunoreactivity. Individual neurons marked by MAP2 staining are indicated (numbers 1–7). (F and G) A subset of SPG49 patient *TECPR2-/-* NGN2 neurons treated with 5 μM lead ASO-005-02 show clear TECPR2 immunoreactivity, indicating rescue of TECPR2 protein expression in the form of TECPR2ΔEx8. These patient-derived neurons positive for TECPR2 signal are indicated by numbers in green in (F). (B–G) Scale bar, 20 μm. (H) Quantification of several FOVs indicates that ~22.5% of SPG49 *TECPR2-/-* patient iPSC neurons exhibited rescue of TECPR2 protein expression in culture, after single treatment (gymnotic delivery) with lead ASO-005-02.

folded, and transported to discrete subcellular domains similar to wild-type, full-length TECPR2.

Further definition of the subcellular structures represented by TECPR2-positive puncta could elucidate neuronal TECPR2 function. Preliminary data using immunocytochemistry for autophagy, ER export, and vesicle-mediated protein trafficking markers suggest involvement of VPS11 (vacuolar protein sorting-associated protein 11 homolog) as a potential TECPR2 interactor, as we observed significant overlap in TECPR2 and VPS11 subcellular localization in human iPSC-derived neurons (Figure S6). We did not detect significant co-localization of TECPR2 with a subset of markers for canonical

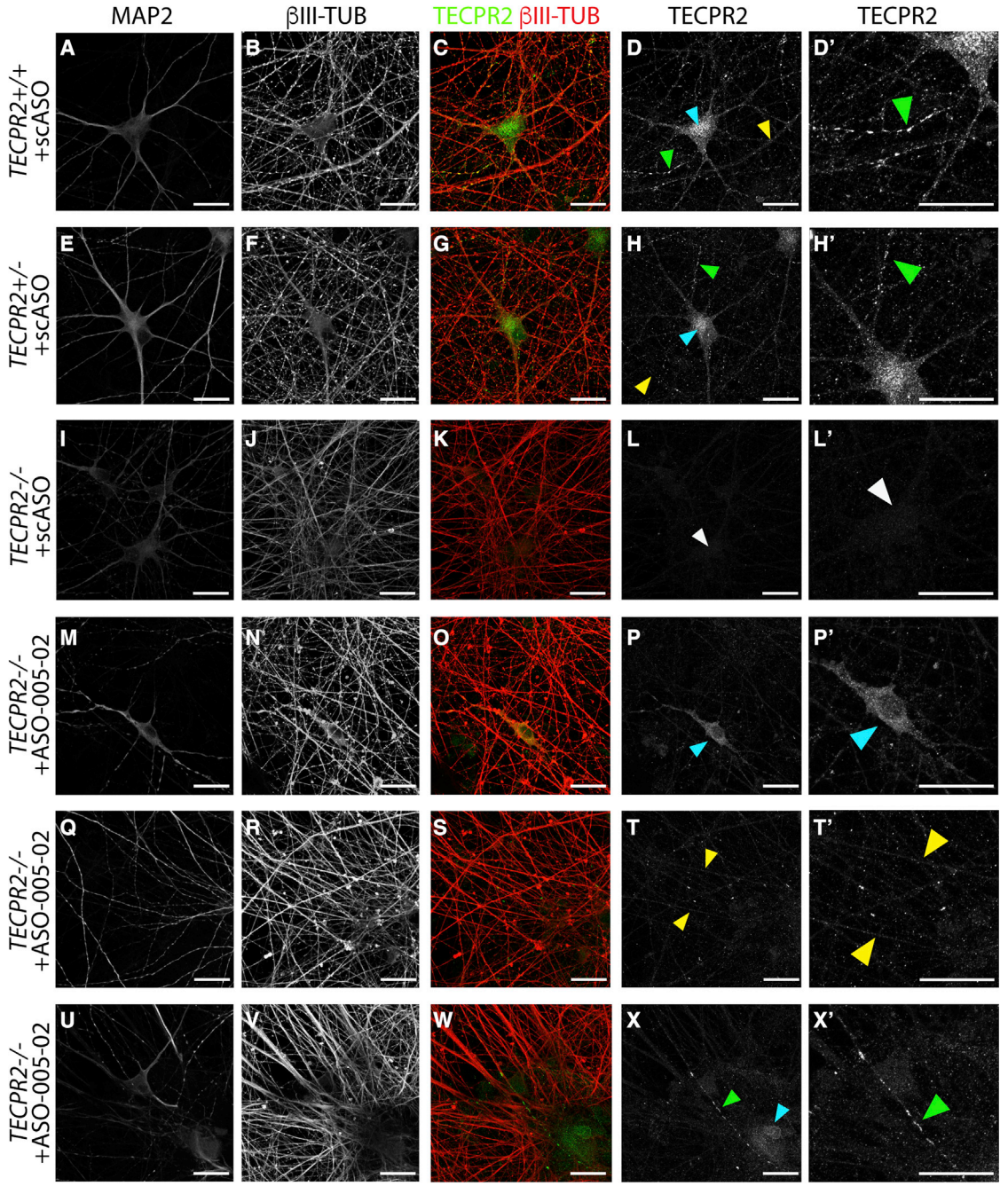

Figure 5. TECPR2 and TECPR2ΔExon8 neuronal localization in patient iPSC-derived neurons

(A–D′) High-resolution immunocytochemistry analyses of control *TECPR2*+/+ iPSC neurons (DIV45) treated with 5 μM scrambled non-targeting negative control ASO (scASO), single dose, gymnotic delivery at plating. Neurons were co-stained for MAP2 (A), β-III TUBULIN (B), and TECPR2 (D). β-III TUBULIN/TECPR2 merged signal (C), and an enlarged (∼2.1×) sub-region of the TECPR2 image (D′) are also presented. Distinct patterns of TECPR2 sub-cellular localization are highlighted in (D) and (D′): broad, speckled puncta pattern within soma and proximal dendrites (cyan arrowhead), small discrete puncta in neurites (yellow arrowhead), and rare large puncta in neurites (green arrowheads). (E–H′) Control *TECPR2*+/- iPSC neurons (DIV45) treated with 5 μM scASO, single dose, gymnotic delivery show similar pattern of TECPR2 subcellular localization to that of *TECPR2*+/+ (D and D′) with the three types of puncta highlighted by arrowheads in (H) and (H′): broad puncta pattern within soma and proximal dendrites (cyan arrowhead), small discrete puncta in neurites (yellow arrowhead), and rare large puncta in neurites (green arrowheads). (I–L′) SPG49 patient *TECPR2*-/- iPSC-derived NGN2 neurons (DIV45) treated with the 5 μM scASO show no TECPR2 immunoreactivity and absence of the punctate expression pattern. White arrowhead in (L) and (L′) indicates lack of TECPR2 immunoreactivity signal in an area of a MAP2+ soma, according to (I). (M–P′) SPG49 patient *TECPR2*-/- iPSC-derived

(legend continued on next page)

endosomal, lysosomal, and autophagosomal compartments in neurons (Figure S7). Furthermore, in initial studies, we did not detect robust alterations in autophagy in patient-derived fibroblasts relative to healthy control fibroblasts (Figure S8) and consequently did not pursue autophagy assays as a basis for further assessment of TECPR2ΔEx8 functionality. In an additional evaluation of functional rescue, preliminary investigation of the interacting partners of TECPR2 and TECPR2ΔEx8 in HEK293 cells using pull-down experiments followed by mass spectrometry-based proteomics suggests that the percentage of retained interactions in these non-neuronal cells ranges from 33% to 72%, depending on the statistical thresholds applied (Figure S9). The evidence that a significant percentage of TECPR2 protein interactions are retained by TECPR2ΔEx8 suggests that TECPR2ΔEx8 may at least partially restore TECPR2 function.

Single-dose tolerability study of lead ASO candidates in cynomolgus monkeys

To determine if the lead ASO candidate ASO-005-02 and two back-up candidates (ASO-059 and ASO-066) have *TECPR2* exon 8-skipping activity *in vivo* and are tolerated in non-human primates, a single-dose (intrathecal; 20 mg) 14-day tolerability study was performed in cynomolgus monkeys (n = 2 per ASO) (Figure 6A). Prior to the *in vivo* study, the efficacy of the ASO candidates was confirmed *in vitro* in cultured cynomolgus monkey fibroblasts using an RT-PCR assay analogous to that used for human fibroblasts (Figure S10). Clinical observations of animals treated with the ASOs indicated that all three ASO candidates had an acceptable tolerability profile with similar non-adverse transient clinical signs and neurological changes (Figure S11). For ASO-005-02, transient behavioral changes included tremors, postural changes, as well as effects on postural reactions and flexor reflexes, which generally resolved by 24 h post dose.

Histopathology analyses of brain, spinal cord (lumbar, thoracic, and cervical), and dorsal root ganglia tissues indicated that the single 20-mg dose of ASO-005-02, ASO-059, or ASO-066 to cynomolgus monkeys via intrathecal injection did not result in any test item-related gross or microscopic changes at study termination (Figure S11). Intrathecal injection resulted in broad uptake of ASO-005-02 in most animals throughout the neuraxis, as measured by hybridization ELISA (Figure 6D). Pharmacodynamic (PD) analyses using RT-PCR in CNS tissues led to the selection of ASO-005-02 as the therapeutic candidate based on its superior *in vivo* *TECPR2* exon 8-skipping activity (Figures 6B and 6C), correlating with ASO concentration in the CNS tissues analyzed (Figure 6D), confirming *in vivo* target engagement via this route of administration. In sum, the single-dose *in vivo* tolerability study indicated that ASO-005-02 is active and has an acceptable tolerability profile when administered by intrathecal injection in cynomolgus monkeys.

DISCUSSION

Here, we report the identification of an ASO therapeutic strategy suitable for patients with an ultra-rare neurological disorder (SPG49) resulting from homozygous truncating mutations in exon 8 of the *TECPR2* gene. The strategy could also benefit patients with the exon 8 mutation in compound heterozygous context. The therapeutic is designed to be administered by intrathecal injection to address the severe, life-threatening neurological symptoms of the disease. The mechanism of action is to induce exon 8 skipping to restore the *TECPR2* mRNA reading frame and induce expression of a form of TECPR2 protein (TECPR2ΔEx8) that lacks 111 amino acids of an apparently unstructured central region of full-length TECPR2.

Following the identification of ASO sequences with *TECPR2* exon 8-skipping activity, optimization studies led to identification of a lead candidate, ASO-005-02, with potent exon 8-skipping activity. Treatment of patient-derived fibroblasts and neurons with ASO-005-02 induced expression of TECPR2ΔEx8 in both patient cell types. TECPR2ΔEx8 protein was shown to retain the distinct, punctate neuronal expression pattern of full-length TECPR2, providing evidence that it is synthesized, folded, and transported to discrete subcellular domains similar to the full-length protein. In addition, preliminary protein interactome studies in HEK293 cells suggest that TECPR2ΔEx8 retains a significant portion of the protein binding interactions of full-length TECPR2. Future interactome studies in human iPSC-derived neurons will be informative to further evaluate TECPR2ΔEx8 in a neuronal context. Based on these observed features of TECPR2ΔEx8, it is anticipated that *TECPR2* exon 8-skipping ASOs may at least partially rescue the function of full-length TECPR2.

Analysis of the effects of exon 8-skipping ASOs in patient-derived cells to confirm and characterize activity in disease-relevant cellular contexts was an important aspect of this study. For these experiments, we utilized dermal fibroblast cells and iPSC-derived neurons from a single SPG49 patient homozygous for the exon 8 *TECPR2* mutation. We were not able to access cell lines from additional patients as a result of the rarity of the disease. However, since the ASO leads target wild-type sequences within the *TECPR2* pre-mRNA and not the patient mutation, we predicted and confirmed exon 8-skipping activity of the candidate ASO in unaffected control cells from different genetic backgrounds (Figure S12). Therefore, we anticipate that the effects of

NGN2 neurons (DIV45) treated with 5 μM ASO-005-02 (single dose, gymnotic delivery at plating) show rescue of broad puncta pattern of TECPR2 expression within soma and proximal dendrites, as highlighted by cyan arrowhead in (P) and enlarged (~2.1×) in (P′). (Q–T′) SPG49 patient *TECPR2-/-* iPSC-derived NGN2 neurons (DIV45) treated with 5 μM ASO-005-02 (single dose, gymnotic delivery at plating) show rescue of expression of small discrete TECPR2-positive puncta in β-III TUBULIN-positive neurites, as highlighted by yellow arrowheads in (T) and enlarged (~2.1×) (T′). (U–X′) SPG49 patient *TECPR2-/-* iPSC-derived NGN2 neurons (DIV45) treated with 5 μM ASO-005-02 (single dose, gymnotic delivery at plating) show rescue of expression of rare large TECPR2-positive puncta in neurites, as highlighted by green arrowhead in (X) and enlarged (~2.1×) (X′). (A–X′) Scale bar, 20 μm.

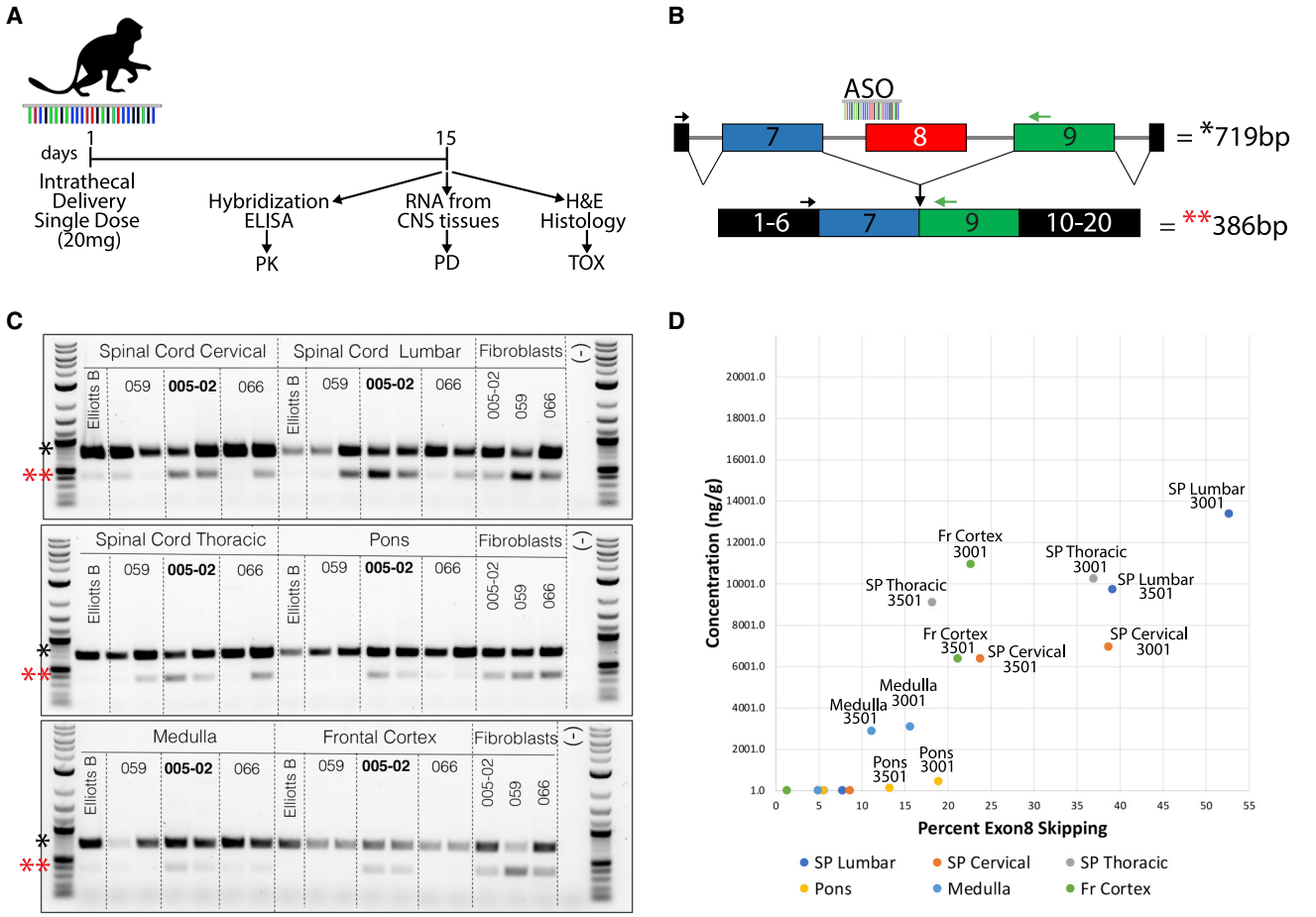

Figure 6. Lead ASO candidate ASO-005-02 is effective in CNS tissues and well tolerated in non-human primates

(A) *In vivo* ASO tolerability study design. A single 20-mg intrathecal dose of each of the three lead ASOs was delivered to cynomolgus monkeys (n = 2 per ASO). Elliotts B solution was used as vehicle control to establish baseline conditions for the different assays. Fourteen days after ASO treatment, animals were necropsied, and different CNS tissues were obtained for pharmacokinetic (PK), pharmacodynamic (PD), and postmortem histopathology analyses. ASO concentrations (ng/g) in the different CNS tissues were determined using a hybridization ELISA assay and percentage of cynomolgus *TECPR2* exon 8 skipping was estimated using a modified version of the patient RT-PCR assay with cynomolgus monkey-specific PCR primers. (B) Diagram of RT-PCR assay for detection of cynomolgus monkey *TECPR2* exon 8 skipping, which corresponds to enrichment of a lower PCR amplicon (~386 bp). (C) DNA gel inverted images showing PCR results for *TECPR2* exon 8-skipping assay for different CNS tissues (spinal cord cervical, lumbar, thoracic, pons, medulla, and frontal cortex) obtained from monkeys treated with each of three ASO leads (ASO-059, ASO-005-02, ASO-066). cDNA samples from cultured monkey fibroblasts transfected with the same three ASOs were used as positive controls for the assay, and molecular biology-grade water (–) was used as negative control for the PCR assay. Significant enrichment of lower PCR amplicon (~386 bp, indicated by red asterisks [**]) can be easily detected for the two animals treated with ASO-005-02, which was selected as the therapeutic candidate based on this superior *in vivo TECPR2* exon 8-skipping activity profile. (D) PK/PD scatterplot showing good correlation between the concentration (ng/g) of ASO-005-02 estimated in different CNS tissues (using hybridization ELISA) and the percentage of *TECPR2* exon 8 skipping (as measured by RT-PCR) detected in those tissues for the two animals (animals 3001 and 3501) treated with this ASO candidate. SP Lumbar, lumbar spinal cord tissue; SP Thoracic, thoracic spinal cord thoracic tissue; Fr Cortex, frontal cortex tissue.

the ASO candidate should generalize to the population of SPG49 patients harboring the exon 8 mutation, which may include up to a few hundred individuals globally, based on estimated mutation carrier frequencies.

Exon-skipping ASO therapeutics that address loss-of-function mutations have been developed for DMD. This strategy led to approval of eteplirsen[22] and golodirsen,[11,23,24] which induce skipping of DMD exons 51 and 53, respectively, rescuing expression of shortened forms of dystrophin lacking the exon-encoded sequences. In-frame deletions including exons 51 or 53 were known to result in Becker muscular dystrophy, a less severe form of muscular dystrophy, providing genetic validation for the ASO therapeutic concept.[25,26] The lack of such genetic concept validation for *TECPR2* exon 8 skipping, and the lack of understanding of TECPR2 function and the SPG49 disease mechanism, present challenges in applying an analogous approach to SPG49. We addressed this by using high-resolution subcellular localization and proteomics studies to identify surrogate

measures of TECPR2 functionality. We propose that the full preservation by TECPR2ΔEx8 of the distinct neuronal subcellular distribution identified for full-length TECPR2 and the partial preservation of its protein interactome are valid surrogates for partial functional restoration.

The distinct neuronal subcellular distribution pattern identified for TECPR2 and its co-localization with VPS11, a core member of CORVET (class C core vacuole/endosome tethering) and HOPS (homotypic fusion and vacuole protein sorting) tethering complexes,[27,28] may shed light on TECPR2 functions relevant to SPG49. Further characterization of the various TECPR2-positive puncta to define these subcellular compartments and investigate how their perturbation could lead to pathogenic manifestations of SPG49 is an important area for future work.

ASO-005-02 employs the same chemical modifications as in nusinersen and was inactive in human peripheral blood mononuclear cell (PBMC) cytokine release assays, suggesting minimal potential for immune stimulatory effects (Figure S13). Finally, a single 20-mg intrathecal dose of ASO-005-02 in cynomolgus monkeys had an acceptable tolerability profile, with some transient non-adverse behavioral effects with no correlating histopathology. The ASO distributed throughout the CNS and induced detectable exon 8 skipping in multiple CNS tissues, demonstrating activity *in vivo* and the applicability of the cynomolgus monkey for assessing toxicology of the candidate. To our knowledge, this is the first report of exon skipping induced in the CNS of non-human primates by an intrathecally administered ASO. Additional long-term toxicology studies in non-human primates across a range of doses with comprehensive toxicology evaluation are needed to gain a complete understanding of the safety profile of this therapeutic candidate and establish whether the candidate has a sufficient therapeutic window to support clinical development. In addition, profiling the effects of the ASO candidate on the transcriptome using RNA sequencing analysis in relevant cellular contexts will be important to examine whether the candidate induces off-target effects at a therapeutically relevant concentration, as potential for off-target effects on transcript expression has been reported for splice-switching ASOs.[29,30] Given the grave prognosis for SPG49 patients, the potential of *TECPR2* exon 8-skipping ASOs to restore TECPR2 expression and function, and the relatively safe profile of this drug class, we expect that this therapeutic approach could ultimately provide clinical benefit to SPG49 patients suffering from *TECPR2* exon 8 mutation-induced disease.

MATERIALS AND METHODS

Derivation and culture of human dermal fibroblast cell lines

Under Institutional Review Board (IRB)-approved protocol and consent forms, we obtained skin punch biopsies from the forearm of an SPG49 patient (*TECPR2-/-*) and from healthy control relatives (*TECPR2+/-* and *TECPR2+/+*). Skin biopsies were cultured using DMEM basal medium (Thermo Fisher Scientific) supplemented with 10% fetal bovine serum (Hyclone FBS Defined (US)-Heat Inactivated) and 1× penicillin:streptomycin solution (Corning), until dermal fibroblast cells expanded and reached 80%–90% confluency in a surface area of ~3.8 cm^2. Fibroblasts were then dissociated with 0.05% Trypsin EDTA (Corning) and passaged by seeding at 1:3 to 1:5 dilution densities. This process was repeated until establishing cryostocks of fibroblasts at passage (P) 3 to 6. All experiments presented here were carried out using fibroblast cells at P6 to P10. Cells were routinely cultured in 96-well Ibidi cell culture clear plates for RT-PCR and immunocytochemistry assays.

Derivation and culture of human iPSC lines and neuronal production

Under IRB-approved protocol and consent forms, we obtained peripheral blood samples (2–4 mL) from an SPG49 patient (*TECPR2-/-*) and from healthy control relatives (*TECPR2+/-* and *TECPR2+/+*). PBMCs were then isolated by density gradient centrifugation with Ficoll. PBMCs were reprogrammed into iPSCs using an established non-integrating method whereby pluripotency-associated factors (OCT4, KLF4, SOX2, and c-Myc) are transiently expressed via Sendai virus particles (Cytotune 2.0 kit, Life Technologies). At least three to five clones per donor were established into iPSC lines, and these cells were routinely expanded in culture and maintained using mTeSR1 medium (STEMCELL Technologies) and cell culture surfaces pre-coated with Matrigel (Corning) according to manufacturers' recommendations. *TECPR2+/+*, *TECPR2+/-*, and *TECPR2-/-* iPSC lines generated as part of this study are available upon reasonable request to the Luke Heller TECPR2 Foundation and Q-State Biosciences. iPSC lines were differentiated into cortical excitatory NGN2 neurons using a transcriptional programming approach, as previously described.[17,18] Briefly, iPSC lines were initially transduced with lentiviral particles expressing the reverse tetracycline transactivator (rtTA) and a tetracycline-responsive (*TetOp*) construct driving the expression of the proneuronal transcription factor Neurogenin-2 (NGN2) and a puromycin antibiotic resistance enzyme. These genetically modified iPSC lines were then expanded in mTeSR1 medium for three to six passages prior to induction of NGN2 expression via doxycycline. For neuronal production, iPSCs were dissociated with Accutase (STEMCELL Technologies) according to manufacturer's recommendations and plated at a density of 300,000 cells/cm^2 using mTeSR1 medium supplemented with 10 μM Rock Inhibitor (Sigma) and 2 μg/mL doxycycline (Sigma) to initiate NGN2 overexpression. A day later, the medium was switched to a 1:1 DMEM/F-12:Neurobasal Medium (Thermo Fisher Scientific) supplemented with 1× GlutaMAX (Life Technologies), 1× non-essential amino acids (Life Technologies), 1× N2 (Gibco), 1× B-27 (Gibco), 2 μg/mL doxycycline (Sigma), and 2 μg/mL puromycin (Sigma). Medium was exchanged daily with fresh medium for three additional days, which then resulted in a highly homogenous population of post-mitotic neurons, which were then dissociated with Accutase and plated at a density of 80,000–100,000 cells/cm^2 onto poly-D-lysine/laminin pre-coated single-well dishes (MatTek) for ASO treatments and immunofluorescence and RT-PCR assays. Human neuronal cultures were seeded and maintained for 30 to 45 days in Neurobasal A Medium supplemented with 1× GlutaMAX (Life Technologies), 1×

non-essential amino acids (Life Technologies), 1× N2 (Gibco), 1× B-27, 10 ng/mL BDNF (R&D), and 10 ng/mL GDNF (R&D). In order to allow for neuronal maturation of the differentiated cells, the cultures were supplemented 3 days after the initial seeding with 40,000 cells/cm^2 of primary mouse cortical glial cells, prepared as previously described.[31]

ASO synthesis and delivery into cultured cells

All ASO molecules used for *in vitro* studies were synthesized (100–250 nmol scale) at Integrated DNA Technologies (IDT) using either 2′-O-methyl or 2′-MOE modified ribonucleosides and phosphorothioate internucleotide linkages. For ASO delivery into human and non-human primate (cynomolgus) fibroblast cells, we used a lipid-based transfection system (Lipofectin, Thermo Fisher Scientific) in which the ASO was incubated with the transfection reagent in Opti-MEM (Themo Fisher Scientific) for 15–20 min prior to the addition of this solution to the cultured cells. For these experiments, we routinely used 0.5 μL of Lipofectin for every 200 μL of cell culture medium, and serum concentration in the medium was reduced from 10% to 2% for the duration of the ASO treatment (typically 3–5 days). For ASO delivery into human iPSC-neuronal cultures, we used gymnotic delivery (no transfection agent) as we observed significant cellular toxicity with lipid-based transfection methods. For gymnotic delivery, the ASO was added to the medium at the desired concentration (typically 2.5 to 5 μM) with a single treatment at the moment of neuronal plating. Medium was exchanged once a week starting 3 days after plating, and ASO was not re-plenished with fresh medium additions.

ASO synthesis and intrathecal delivery into non-human primates

For *in vivo* studies, the top three lead ASOs: ASO-059, ASO-005-02, and ASO-066, were re-synthesized at the 1.1 g scale at Axolabs (Germany) and additional quality control was carried out on these production batches with acceptable endotoxin levels (<0.10 EU/mg). The new corresponding production identity numbers (IDs) for these three new batches of ASOs were QS0321489-05 (same sequence as ASO-059 and also designated in some figures as 89-05), QS0321490-05 (same sequence as ASO-005-02 and also designated in some figures as 90-05), and QS0321491-05 (same sequence as ASO-066 and also designated in some figures as 91-05). ASO *in vivo* work was carried out at Charles River Laboratories (Charles River Laboratories Montreal ULC; Senneville Site) under their Institutional Animal Care and Use Committee (IACUC)-approved protocols. Briefly, ASOs as lyophilized powders were dissolved in Elliotts B solution at 20 mg/mL and sterile filtered using a 0.22-μm PVDF membrane. Animals were dosed under general anesthesia in lateral recumbency position by direct intrathecal puncture at the lumbar level using a spinal needle. Dosing volume was 1 mL, followed by a 0.25-mL flush of Elliotts B solution. The term of the study was 2 weeks, at which point animals were euthanized, and necropsy and terminal analyses performed. Endpoints evaluated in the study included mortality, clinical observations, body weights, neurological examinations, cerebrospinal fluid (CSF) and tissue bioanalysis for ASO concentration by hybridization ELISA (samples collected at necropsy), tissue *TECPR2* mRNA splicing analysis by RT-PCR, gross necropsy findings, and histopathological examinations. At study termination, CNS tissues, CSF, and liver and kidney tissues were collected for the pharmacokinetic (tissue bioanalysis) and pharmacodynamic (*TECPR2* exon 8-skipping RT-PCR assay) analyses. ASO concentrations in tissues were determined by hybridization ELISA (HELISA) using a dual probe capture/detection method as previously reported.[32] The HELISA quantification method for ASO-005-02, ASO-059, and ASO-066 used a capture probe that consisted of sequence GTCTGGATG linked to biotin at the 3′ end and a detection probe that consisted of sequence TCTGGAGAT linked to digoxigenin at the 5′ end, and the method was further optimized and validated as a qualified analytical procedure at Charles River Laboratories (Montreal). The *TECPR2* exon 8-skipping RT-PCR assay for PD analyses is described next.

RT-PCR (*TECPR2* exon 8 skipping) assays

For RT-PCR exon 8-skipping assay, two different methods were used for RNA and cDNA preparations, depending on the initial source (cultured cells versus *in vivo* tissues). For cultured fibroblasts, total RNA was initially prepared 3–5 days after ASO treatment using the RNA lysis reagents from the Cell-to-C_T kit (Thermo Fisher Scientific), following manufacturer's recommendations, and a total of 50 μL of lysis solution (containing DNase I) per cell culture well. cDNA for these RNA samples was prepared in a 50-μL volume using the RT reagents of the same kit, 10 μL of lysed sample, and following manufacturer's RT protocol (37°C 1 h, 95°C 5min). cDNA was then diluted 1:2 to 1:10 in molecular biology-grade nuclease-free water prior to setting up PCR assays. For tissue samples from the *in vivo* study, tissue was homogenized, and total RNA was obtained using the RiboPure RNA Purification kit (Thermo Fisher Scientific). For this particular set of samples, RNA was quantified using a Nanodrop and was diluted to 10 ng/μL in nuclease-free water prior to cDNA synthesis. This purified total RNA was reverse transcribed to cDNA using iScript Reverse Transcription Supermix (Bio-Rad Laboratories) with 100 ng (10 μL) of the RNA template and combined oligo(dT) and random primers according to the manufacturer's protocol: priming at 25°C for 5 min, RT at 46°C for 20 min, and RT inactivation at 95°C for 1 min. The resulting cDNA was then diluted 1:2 to 1:10 in nuclease-free water. All PCR assays were carried out in 96-well plates using a Mastercycler Pro S Thermocycler 6325 (Eppendorf). PCR-based *TECPR2* exon 8-skipping assays used a 25-μL reaction containing KOD Hot Start Master Mix (Sigma), 400 nM solutions of each of two primers, and 10 μL of diluted cDNA sample. The following primer pairs were used on human and non-human primate samples, respectively: human *TECPR2* forward primer #25 (GGGACTGTT CAAGCCACGTTTATC) and human *TECPR2* reverse primer #30 (AAATTCGGAGCAGGGTGTCGATTC); cynomolgus *TECPR2* forward primer #96 (AGATGCTTTTGCCGGGGGAGTC) and cynomolgus *TECPR2* reverse primer #97 (GGGGACTGTCCCCAGGA AAT). PCR amplification protocol consisted of the following steps: 95°C for 2 min, 35× (95°C for 20 s, 58°C for 10 s, 70°C for 30 s), and 70°C for 5 min. RT-PCR products were resolved using electrophoresis with 1% agarose gel stained with SYBR Safe DNA Gel Stain (Thermo Fisher Scientific) and visualized with a Chemidoc Touch

Imaging System (Bio-Rad Laboratories). A 1-kb DNA ladder (New England Biolabs #N0550S) was loaded into each gel row to serve as a marker for the size of the *TECPR2* PCR products. A PCR sample showing successful *TECPR2* exon 8 skipping appears as enrichment of a lower-molecular-weight PCR product (reduced by 333 bp) in comparison with the upper PCR band, which includes exon 8 (wild type or full-length *TECPR2* product). In order to quantify the percentage of *TECPR2* exon8-skipped product and wild-type TECPR2 product, the intensities of the PCR bands were evaluated using Image Lab software (Bio-Rad Laboratories). The output of this algorithm is designated as "adj volume" and represents the adjusted volume of each band after background subtraction. After adjusted volumes are calculated for the PCR bands present on a gel, the sum of the total adj volume for all PCR bands in a sample is designated as 1.00 and the contribution of the two PCR bands (full-length *TECPR2* versus *TECPR2ΔExon8*) to this sum is expressed as percentages, by dividing the adj volume for each PCR band by the sum and then multiplying by 100.

Immunocytochemistry assays

Immunocytochemistry (ICC) assays were carried out as previously reported.[18] Briefly, fibroblast and neuronal cultures were fixed using 4% paraformaldehyde diluted in 1× PBS from a 16% aqueous solution (Electron Microscopy Sciences) for 20 min and then permeabilized with 0.2% Triton X-100 (Sigma). Cell culture dishes were blocked with 10% donkey serum in 0.1% PBS-Tween for 1 h and then incubated with primary antibodies overnight at 4°C. After five washes with 0.1% PBS-Tween, dishes were treated with secondary (Alexa -conjugated) antibodies for 1 h at room temperature. Cell nuclei (DNA) were stained with Hoechst 33342. Primary antibodies used in this study were the cytoskeletal pan-neuronal markers MAP2 (Abcam; ab5392, 1:3,000) and β-III TUBULIN (TUJ1, BioLegend; #801202, 1:1,000), custom rabbit polyclonal antibody against TECPR2[4] 1:300 (produced in the laboratory of Dr. Christian Behrends), VPS11 (Santa Cruz; sc-515094, 1:300). For fibroblast cultures in 96-well Ibidi plates, images were acquired as maximum-intensity Z-projections using the automated confocal microscope GE Healthcare IN Cell Analyzer 6000 with 20× (0.75NA) objective. Single-cell TECPR2 expression in fibroblasts was estimated using a custom automated microscopy pipeline. Briefly, cell nuclei were first identified via histogram splitting on preprocessed images from the Hoechst33342 channel, with a second pass via a local watershed algorithm to split nuclei detected as possibly fused. Nuclear segmentations for each field were manually appraised and rejected in cases of gross proliferation or poor segmentations. Individual nuclei were then subjected to algorithmic quality criteria assessing size, eccentricity, snowiness, solidity, and average Hoechst33342 brightness (to catch fluorescent artifacts). As the TECPR2 staining pattern was expected to be punctate, fluorescence values from the TECPR2 channel were captured using a 20-pixel halo that was drawn around each annotated cell nucleus, with duplicate claims on specific pixels resolved via nearest neighbors. For statistical analysis, we carried out a one-way ANOVA followed by pairwise t tests to evaluate differences between the five groups. p values were false discovery rate (FDR) corrected to account for multiple hypothesis testing. Analysis was performed in R (version 3.6.3). For human neuronal cultures treated with ASOs, ICC images were acquired using the LSM880 confocal microscope with 60× objective.

Autophagy and immunoblotting assays

Autophagy assays with Bafilomycin A1 were carried out as previously described.[33] For detection of protein levels using immunoblotting assays, protein concentrations were determined using BCA assay on a Nanodrop, and 10–30 μg of protein sample were loaded and separated using SDS-PAGE. After protein transfer onto membranes, these were incubated with primary antibodies overnight and corresponding HRP-conjugated secondary antibodies for 1–2 h prior to developing and measuring protein signal. Primary antibodies and dilution used were MAP1LC3B (Cell Signaling Technology 2775, 1:500 dilution), SQSTM1 (Cell Signaling Technology 5114S, 1:500 dilution), GAPDH (Abcam ab9484, 1:2,000 dilution), and custom rabbit polyclonal antibody against TECPR2[4] 1:300 (produced in the laboratory of Dr. Christian Behrends).

Human PBMC assays

Human PBMC assays were carried out at Axolabs (Germany). Starting material for human PBMCs was buffy coat blood corresponding to 500 mL of full-blood transfusion units. Each unit was obtained from healthy volunteers, and glucose-citrate was used as anti-agglutinant. Initial buffy coat volume was 28–32 mL, and the sealed bag was opened about 40 h after blood donation, when isolation of human PBMCs was carried out via Ficoll gradient centrifugation. PBMCs were resuspended in 10 mL of RPMI1640 complete medium (1× L-glutamine, 1× penicillin-streptomycin (Pen/Strep), and 10% fetal calf serum). PBMCs were seeded at 100,000 cells/well of 96-well cell culture plates in 100 μL of complete medium and maintained inside a 37 °C/5% CO_2 incubator. ASO molecules (ASO-005-02, ASO-059, and ASO-066) were delivered at three different concentrations (50 nM, 150 nM, 300 nM) using lipid-based transfection via OptiMem and Lipofectamine 2000 (0.5 mL/well). Twenty-four hours after transfection and incubation (37°C/5% CO_2), multiple cytokines (interferon [IFN]-α2a, IFN-β, interleukin [IL]-1β, IL-6, tumor necrosis factor [TNF]-α) were measured and analyzed via the MSD platform. Multiple positive controls (inflammatory stimuli) were used, including a TLR7/8 agonist (XD-01024, a cholesterol-conjugated ApoB siRNA); a TLR9 agonist (ODN2216, a 20-mer CpG oligo containing unmethylated CpG); a TLR7/8 agonist (XD-00366, a 25-mer double-stranded, unmodified, blunt-ended LacZ RNA duplex); and a TLR3, RIG-I/MDA5, and PKR agonist (low-molecular-weight polyinosinic-polycytidylic acid [LMW poly(I:C)]). A chemically modified siRNA (XD-03999) against factor VII (FVII) was used as negative control.

TECPR2 interactome studies in HEK cell lines

HEK293 *TECPR2*-/- cells were generated by CRISPR-Cas9 gene editing followed by clonal selection. A stable *TECPR2*-/- HEK293 line was generated and shown to have no TECPR2 protein expression by immunocytochemistry with the anti-TECPR2 antibody. The

TECPR2-/- HEK293 cell line was separately transfected with expression constructs for hemagglutinin (HA)-tagged TECPR2 and HA-tagged TECPR2ΔEx8, and stable clones selected and expanded. The following four resulting cell lines were used for the pull-down experiment: (1) *TECPR2-/-* HEK293-HA-TECPR2 (*TECPR2/-* stably expressing full-length HA-TECPR2), (2) *TECPR2-/-* HEK293-HA-TECPR2ΔEx8 (*TECPR2-/-* stably expressing HA-TECPR2ΔEx8), (3) *TECPR2-/-* HEK293-non-transfected (negative control for anti-HA pull-down), (4) *TECPR2+/+* parental HEK293-non-transfected (negative control for anti-HA pull-down). Eight replicates of each of the four cell lines were used for pull-down experiments for a total of 32. The combination of the stable HA-tagged bait expression protocol with the large number of replicates provided an optimal design and well-powered experiment for detecting potential interactors of the two forms of TECPR2 in the HEK293 cellular background. Cells were grown to 75% confluency, and protein lysates were generated. Pull-downs were performed using beads conjugated to anti-HA antibody, followed by extensive washing of beads. Pulled down proteins were eluted by adding an excess of HA-tagged peptide to the beads and isolating the supernatant. The eluted protein samples were analyzed by mass-spectrometry-based proteomics analysis. Proteome informatics results and protein database FASTA files including spectral count data were provided to A2Idea (Ann Arbor, MI) for statistical analysis to define significant interactors. Prior to statistical analysis, proteins commonly observed in affinity-purification coupled to mass spectrometry (AP-MS) experimental blanks were identified in and removed from all comparisons. These proteins represent non-specific binding to the assay antibody used (anti-HA-tag) and must be removed from any label-free analysis as they do not represent a true interaction. The non-specific binding proteins were identified using a public database resource for AP-MS (crapome.org) that enables users to download lists of common contaminants in AP-MS experiments.[34] Four replicate experiments using the HA-tag were downloaded from crapome. All proteins found in common among these four experiments were taken to be contaminants. Any occurrence of these proteins was removed from the spectral count data prior to running significance analysis. Significant interactors were identified using the significance analysis of interactome (SAINT) algorithm,[35] a computational tool that assigns confidence scores to protein-protein interaction data generated using AP-MS. The method utilizes label-free quantitative data (i.e., spectral counts). Using spectral counts, SAINT constructs separate distributions for true and false interactions to derive the probability of a *bona fide* protein-protein interaction. A stringent Bayesian FDR (BFDR) of 0.01 statistical threshold was used to define interactors. Log of odds ratios (LORs) of 40, 30, and 20 were applied to the identified interactors to define likely significant interaction candidates over a range of statistical thresholds.

Data availability

The most relevant datasets generated and analyzed as part of this study are included in this published article (and its supplementary information files). Additional data analyzed in the study are available from the corresponding authors on reasonable request. Custom code used for the automated microscopy pipeline is restricted from outside use.

SUPPLEMENTAL INFORMATION

Supplemental information can be found online at https://doi.org/10.1016/j.omtn.2022.06.015.

ACKNOWLEDGMENTS

The project was funded by the TECPR2 Foundation. We would like to thank Dr. Charles Berde and Dr. Robert J. Graham at Boston Children's Hospital for their insights on preclinical *in vivo* studies.

AUTHOR CONTRIBUTIONS

G.T.D, A.K., L.A.W., D.J.G., A.E., W.C.T., and D.M. designed ASO strategy. L.A.W. and W.C.T. designed all *in vitro* ASO experiments in fibroblasts and human iPSC neurons. W.C.T., V.J., S.H.R., H.S., and L.A.W. executed ASO experiments in fibroblasts. V.B. carried out immunocytochemistry (ICC) assays. N.D.B. developed qICC pipeline for fibroblast assays. K.H. and H.U. carried out iPSC-neuronal production and cultures. V.J., A.D., and J.M. carried out TECPR2 immunoblotting assays. S.J.R., C.L., and N.D.B. assisted with data analyses. L.B., J.D., and S.C. supervised and carried out behavioral studies in cynomolgus monkeys. H.L. carried out HELISA assays. C.A., G.M., H.S., and L.A.W. executed PD RT-PCR assays in non-human primate mRNA samples. A.S. and L.G. carried out autophagy assays. C.B. assisted with validation of *TECPR2* immunoreagents. K.N. and C.B. carried out interactome experiments in HEK293 cells. T.W.Y. carried out initial genotyping of *TECPR2* mutation in the SPG49 patient. C.L., D.B., and S.A. designed ASO sequences. L.W., D.J.G., A.E., A.K., and G.T.D. provided scientific oversight over interpretation of experimental results and wrote the manuscript.

DECLARATION OF INTERESTS

We declare that one or more of the authors have a competing interest: L.A.W., D.J.G., A.E., V.B., N.D.B., C.A., G.M., V.J., H.S., K.H., H.U., S.H.R., A.D., J.M., S.J.R., C.L., S.A., D.M., and G.T.D. are employees or consultants of Q-State Biosciences and hold stock.

REFERENCES

1. Oz-Levi, D., Ben-Zeev, B., Ruzzo, E.K., Hitomi, Y., Gelman, A., Pelak, K., Anikster, Y., Reznik-Wolf, H., Bar-Joseph, I., Olender, T., et al. (2012). Mutation in TECPR2 reveals a role for autophagy in hereditary spastic paraparesis. Am. J. Hum. Genet. *91*, 1065–1072. https://doi.org/10.1016/j.ajhg.2012.09.015.

2. Heimer, G., Oz-Levi, D., Eyal, E., Edvardson, S., Nissenkorn, A., Ruzzo, E.K., Szeinberg, A., Maayan, C., Mai-Zahav, M., Efrati, O., et al. (2016). TECPR2 mutations cause a new subtype of familial dysautonomia like hereditary sensory autonomic neuropathy with intellectual disability. Eur. J. Paediatr. Neurol. *20*, 69–79. https://doi.org/10.1016/j.ejpn.2015.10.003.

3. Patwari, P.P., Wolfe, L.F., Sharma, G.D., and Berry-Kravis, E. (2020). TECPR2 mutation-associated respiratory dysregulation: more than central apnea. J. Clin. Sleep Med. *16*, 977–982. https://doi.org/10.5664/jcsm.8434.

4. Stadel, D., Millarte, V., Tillmann, K.D., Huber, J., Tamin-Yecheskel, B.C., Akutsu, M., Demishtein, A., Ben-Zeev, B., Anikster, Y., Perez, F., et al. (2015). TECPR2 cooperates with LC3C to regulate COPII-dependent ER export. Mol. Cell *60*, 89–104. https://doi.org/10.1016/j.molcel.2015.09.010.

5. Behrends, C., Sowa, M.E., Gygi, S.P., and Harper, J.W. (2010). Network organization of the human autophagy system. Nature *466*, 68–76. https://doi.org/10.1038/nature09204.

6. Fraiberg, M., Tamim-Yecheskel, B.C., Kokabi, K., Subic, N., Heimer, G., Eck, F., Nalbach, K., Behrends, C., Ben-Zeev, B., Shatz, O., et al. (2021). Lysosomal targeting of autophagosomes by the TECPR domain of TECPR2. Autophagy *17*, 3096–3108. https://doi.org/10.1080/15548627.2020.1852727.

7. Hahn, K., Rohdin, C., Jagannathan, V., Wohlsein, P., Baumgärtner, W., Seehusen, F., Spitzbarth, I., Grandon, R., Drögemüller, C., and Jäderlund, K.H. (2015). TECPR2 associated neuroaxonal dystrophy in Spanish water dogs. PLoS One *10*, e0141824. https://doi.org/10.1371/journal.pone.0141824.

8. Tamim-Yecheskel, B.-C., Fraiberg, M., Kokabi, K., Freud, S., Shatz, O., Marvaldi, L., Subic, N., Brenner, O., Tsoory, M., Eilam-Altstadter, R., et al. (2021). A tecpr2 knockout mouse exhibits age-dependent neuroaxonal dystrophy associated with autophagosome accumulation. Autophagy *17*, 3082–3095. https://doi.org/10.1080/15548627.2020.1852724.

9. Li, D., Mastaglia, F.L., Fletcher, S., and Wilton, S.D. (2018). Precision medicine through antisense oligonucleotide-mediated exon skipping. Trends Pharmacol. Sci. *39*, 982–994. https://doi.org/10.1016/j.tips.2018.09.001.

10. Wilton, S.D., Lloyd, F., Carville, K., Fletcher, S., Honeyman, K., Agrawal, S., and Kole, R. (1999). Specific removal of the nonsense mutation from the mdx dystrophin mRNA using antisense oligonucleotides. Neuromuscul. Disord. *9*, 330–338. https://doi.org/10.1016/s0960-8966(99)00010-3.

11. Charleston, J.S., Schnell, F.J., Dworzak, J., Donoghue, C., Lewis, S., Chen, L., Young, G.D., Milici, A.J., Voss, J., DeAlwis, U., et al. (2018). Eteplirsen treatment for Duchenne muscular dystrophy: exon skipping and dystrophin production. Neurology *90*, e2146–e2154. https://doi.org/10.1212/wnl.0000000000005680.

12. Ottesen, E.W. (2017). ISS-N1 makes the first FDA-approved drug for spinal muscular atrophy. Transl. Neurosci. *8*, 1–6. https://doi.org/10.1515/tnsci-2017-0001.

13. Parente, V., and Corti, S. (2018). Advances in spinal muscular atrophy therapeutics. Ther. Adv. Neurol. Disord. *11*. 175628561875450. https://doi.org/10.1177/1756285618754501.

14. Bennett, C.F., Kordasiewicz, H.B., and Cleveland, D.W. (2021). Antisense drugs make sense for neurological diseases. Annu. Rev. Pharmacol. Toxicol. *61*, 831–852. https://doi.org/10.1146/annurev-pharmtox-010919-023738.

15. Neuser, S., Brechmann, B., Heimer, G., Brösse, I., Schubert, S., O'grady, L., Zech, M., Srivastava, S., Sweetser, D.A., Houlden, H., et al. (2021). Clinical, neuroimaging, and molecular spectrum of TECPR2-associated hereditary sensory and autonomic neuropathy with intellectual disability. Hum. Mutat. *42*, 762–776.

16. Roberts, T.C., Langer, R., and Wood, M.J.A. (2020). Advances in oligonucleotide drug delivery. Nat. Rev. Drug Discov. *19*, 673–694. https://doi.org/10.1038/s41573-020-0075-7.

17. Zhang, Y., Pak, C., Han, Y., Ahlenius, H., Zhang, Z., Chanda, S., Marro, S., Patzke, C., Acuna, C., Covy, J., et al. (2013). Rapid single-step induction of functional neurons from human pluripotent stem cells. Neuron *78*, 785–798. https://doi.org/10.1016/j.neuron.2013.05.029.

18. Williams, L.A., Joshi, V., Murphy, M., Ferrante, J., Werley, C.A., Brookings, T., McManus, O., Grosse, J., Davies, C.H., and Dempsey, G.T. (2019). Scalable measurements of intrinsic excitability in human iPS cell-derived excitatory neurons using all-optical electrophysiology. Neurochem. Res. *44*, 714–725. https://doi.org/10.1007/s11064-018-2694-5.

19. Jafar-Nejad, P., Powers, B., Soriano, A., Zhao, H., Norris, D.A., Matson, J., DeBrosse-Serra, B., Watson, J., Narayanan, P., Chun, S.J., et al. (2021). The atlas of RNase H antisense oligonucleotide distribution and activity in the CNS of rodents and non-human primates following central administration. Nucleic Acids Res. *49*, 657–673. https://doi.org/10.1093/nar/gkaa1235.

20. Hori, S.I., Yamamoto, T., Waki, R., Wada, S., Wada, F., Noda, M., and Obika, S. (2015). Ca2+ enrichment in culture medium potentiates effect of oligonucleotides. Nucleic Acids Res. *43*, e128. https://doi.org/10.1093/nar/gkv626.

21. Shen, X., Beasley, S., Putman, J.N., Li, Y., Prakash, T.P., Rigo, F., Napierala, M., and Corey, D.R. (2019). Efficient electroporation of neuronal cells using synthetic oligonucleotides: identifying duplex RNA and antisense oligonucleotide activators of human frataxin expression. RNA *25*, 1118–1129. https://doi.org/10.1261/rna.071290.119.

22. Lim, K.R.Q., Maruyama, R., and Yokota, T. (2017). Eteplirsen in the treatment of Duchenne muscular dystrophy. Drug Des. Dev. Ther. *11*, 533–545. https://doi.org/10.2147/dddt.s97635.

23. Heo, Y.A. (2020). Golodirsen: first approval. Drugs *80*, 329–333.

24. Frank, D.E., Schnell, F.J., Akana, C., El-Husayni, S.H., Desjardins, C.A., Morgan, J., Charleston, J.S., Sardone, V., Domingos, J., Dickson, G., et al. (2020). Increased dystrophin production with golodirsen in patients with Duchenne muscular dystrophy. Neurology *94*, e2270–e2282. https://doi.org/10.1212/wnl.0000000000009233.

25. Anthony, K., Cirak, S., Torelli, S., Tasca, G., Feng, L., Arechavala-Gomeza, V., Armaroli, A., Guglieri, M., Straathof, C.S., Verschuuren, J.J., et al. (2011). Dystrophin quantification and clinical correlations in Becker muscular dystrophy: implications for clinical trials. Brain *134*, 3547–3559. https://doi.org/10.1093/brain/awr291.

26. Waldrop, M.A., Yaou, R.B., Lucas, K.K., Martin, A.S., O'Rourke, E., Ferlini, A., Ferlini, A., Muntoni, F., Leturcq, F., Weiss, R.B., et al. (2020). Clinical phenotypes of DMD exon 51 skip equivalent deletions: a systematic review. J. Neuromuscul. Dis. *7*, 217–229. https://doi.org/10.3233/jnd-200483.

27. Van Der Kant, R., Jonker, C.T.H., Wijdeven, R.H., Bakker, J., Janssen, L., Klumperman, J., and Neefjes, J. (2015). Characterization of the mammalian CORVET and HOPS complexes and their modular restructuring for endosome specificity. J. Biol. Chem. *290*, 30280–30290. https://doi.org/10.1074/jbc.m115.688440.

28. Balderhaar, H.J. klein., and Ungermann, C. (2013). CORVET and HOPS tethering complexes - coordinators of endosome and lysosome fusion. J. Cell Sci. *126*, 1307–1316. https://doi.org/10.1242/jcs.107805.

29. Scharner, J., Ma, W.K., Zhang, Q., Lin, K.-T., Rigo, F., Bennett, C.F., and Krainer, A.R. (2020). Hybridization-mediated off-target effects of splice-switching antisense oligonucleotides. Nucleic Acids Res. *48*, 802–816. https://doi.org/10.1093/nar/gkz1132.

30. Ottesen, E.W., Luo, D., Singh, N.N., and Singh, R.N. (2021). High concentration of an iss-n1-targeting antisense oligonucleotide causes massive perturbation of the transcriptome. Int. J. Mol. Sci. *22*, 8378. https://doi.org/10.3390/ijms22168378.

31. Di Giorgio, F.P., Boulting, G.L., Bobrowicz, S., and Eggan, K.C. (2008). Human embryonic stem cell-derived motor neurons are sensitive to the toxic effect of glial cells carrying an ALS-causing mutation. Cell Stem Cell *3*, 637–648. https://doi.org/10.1016/j.stem.2008.09.017.

32. Efler, S.M., Zhang, L., Noll, B.O., Uhlmann, E., and Davis, H.L. (2005). Quantification of oligodeoxynucleotides in human plasma with a novel hybridization assay offers greatly enhanced sensitivity over capillary gel electrophoresis. Oligonucleotides *15*, 119–131. https://doi.org/10.1089/oli.2005.15.119.

33. Yamazaki, T., Kirchmair, A., Sato, A., Buqué, A., Rybstein, M., Petroni, G., Bloy, N., Finotello, F., Stafford, L., Navarro Manzano, E., et al. (2020). Mitochondrial DNA drives abscopal responses to radiation that are inhibited by autophagy. Nat. Immunol. *21*, 1160–1171. https://doi.org/10.1038/s41590-020-0751-0.

34. Mellacheruvu, D., Wright, Z., Couzens, A.L., Lambert, J.P., St-Denis, N.A., Li, T., Miteva, Y.V., Hauri, S., Sardiu, M.E., Low, T.Y., et al. (2013). The CRAPome: a contaminant repository for affinity purification-mass spectrometry data. Nat. Methods *10*, 730–736. https://doi.org/10.1038/nmeth.2557.

35. Choi, H., Larsen, B., Lin, Z.Y., Breitkreutz, A., Mellacheruvu, D., Fermin, D., Qin, Z.S., Tyers, M., Gingras, A.C., and Nesvizhskii, A.I. (2011). SAINT: probabilistic scoring of affinity purification–mass spectrometry data. Nat. Methods *8*, 70–73. https://doi.org/10.1038/nmeth.1541.

OMTN, Volume *29*

Supplemental information

Developing antisense oligonucleotides for a *TECPR2* mutation-induced, ultra-rare neurological disorder using patient-derived cellular models

Luis A. Williams, David J. Gerber, Amy Elder, Wei Chou Tseng, Valeriya Baru, Nathaniel Delaney-Busch, Christina Ambrosi, Gauri Mahimkar, Vaibhav Joshi, Himali Shah, Karthiayani Harikrishnan, Hansini Upadhyay, Sakthi H. Rajendran, Aishwarya Dhandapani, Joshua Meier, Steven J. Ryan, Caitlin Lewarch, Lauren Black, Julie Douville, Stefania Cinquino, Helen Legakis, Karsten Nalbach, Christian Behrends, Ai Sato, Lorenzo Galluzzi, Timothy W. Yu, Duncan Brown, Sudhir Agrawal, David Margulies, Alan Kopin, and Graham T. Dempsey

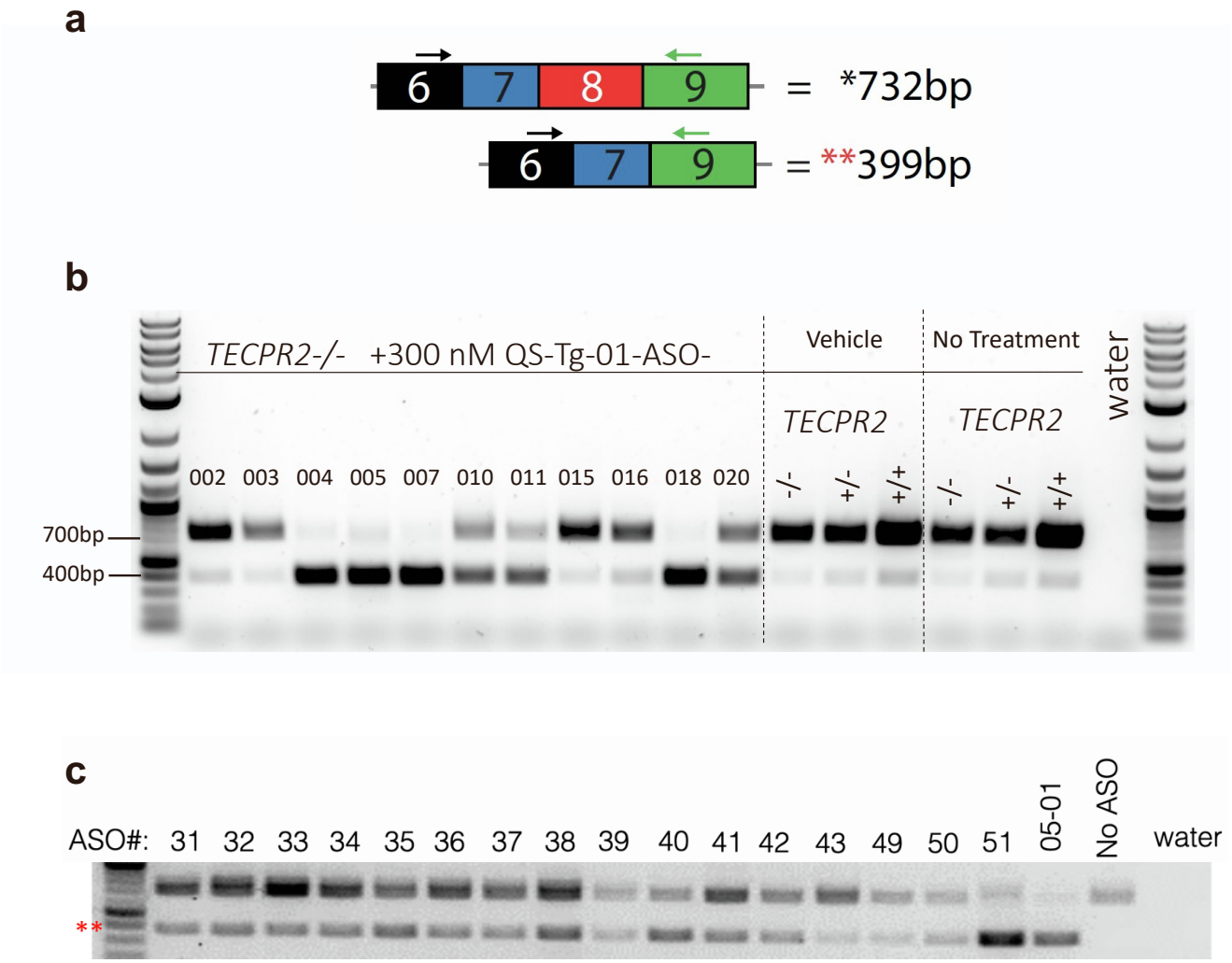

Supplementary Figure 1: Subsequent ASO screening with optimized experimental conditions and additional ASO tiling experiments. **a**, Diagram of RT-PCR assay and PCR amplicons to be obtained when *TECPR2* exon 8 is skipped in human fibroblasts. **b**, Additional ASO screening assay using reduced ASO concentration (300 nM versus 1 μM) and increased incubation time (120 hours versus 72 hours) identified active ASOs targeting the 3' end of *TECPR2* Exon 8 (ASO-018 and ASO-020). cDNA from *TECPR2-/-*, *TECPR2+/-* and *TECPR2+/+* fibroblasts treated with vehicle only (transfection reagent) or exposed to no treatment were used as negative controls. Significant enrichment of lower PCR product (~399bp,**), corresponding to *TECPR2ΔExon8* transcript, can be detected in samples from fibroblasts treated with ASO-004, ASO-005, ASO-007, ASO-010, ASO-011, ASO-018 and ASO-020. **c**, PCR results from additional ASO tiling experiments (1 μM ASO treatment for 72 hours) in TECPR2-/- patient fibroblasts covering the *TECPR2* region homologous to Cynomolgus *TECPR2* within the initially identified positive region for ASO-mediated Exon 8 skipping.

ASO ID	Length (mer)	ASO Sequence (5' to 3')
ASO-020	25	GCTACAGAGGGTACCTGTCTTCTTC
ASO-021	25	AGACATCTCCAGACCATCTCTCACT
ASO-022	25	CCAGACATCTCCAGACCATCTCTCA
ASO-023	25	ACATCTCCAGACCATCTCTCACTAA
ASO-024	25	ATCTCCAGACCATCTCTCACTAAGA
ASO-025	18	CCAGACCAUCUCUCACUA
ASO-026	18	UCCAGACCAUCUCUCACU
ASO-027	18	CUCCAGACCAUCUCUCAC
ASO-028	18	UCUCCAGACCAUCUCUCA
ASO-029	18	AUCUCCAGACCAUCUCUC
ASO-030	18	CAUCUCCAGACCAUCUCU
ASO-031	18	ACAUCUCCAGACCAUCUC
ASO-032	18	GACAUCUCCAGACCAUCU
ASO-033	18	AGACAUCUCCAGACCAUC
ASO-034	18	CAGACAUCUCCAGACCAU
ASO-035	18	CCAGACAUCUCCAGACCA
ASO-036	18	UCCAGACAUCUCCAGACC
ASO-037	18	AUCCAGACAUCUCCAGAC
ASO-038	18	CAUCCAGACAUCUCCAGA
ASO-039	18	GCAUCCAGACAUCUCCAG
ASO-040	18	AGCAUCCAGACAUCUCCA
ASO-041	18	GAGCAUCCAGACAUCUCC
ASO-042	18	UGAGCAUCCAGACAUCUC
ASO-043	18	CUGAGCAUCCAGACAUCU
ASO-044	18	UCUGAGCAUCCAGACAUC
ASO-045	18	CUCUGAGCAUCCAGACAU
ASO-046	18	GCUCUGAGCAUCCAGACA
ASO-047	18	CGCUCUGAGCAUCCAGAC
ASO-048	21	UCUCCAGACCAUCUCUCACUA
ASO-049	21	AUCUCCAGACCAUCUCUCACU
ASO-050	21	CAUCUCCAGACCAUCUCUCAC
ASO-051	21	ACAUCUCCAGACCAUCUCUCA
ASO-052	21	GACAUCUCCAGACCAUCUCUC
ASO-053	21	CAGACAUCUCCAGACCAUCUC
ASO-054	21	CCAGACAUCUCCAGACCAUCU
ASO-055	21	UCCAGACAUCUCCAGACCAUC
ASO-056	21	AUCCAGACAUCUCCAGACCAU
ASO-057	21	CAUCCAGACAUCUCCAGACCA
ASO-058	21	AGCAUCCAGACAUCUCCAGAC
ASO-059	21	GAGCAUCCAGACAUCUCCAGA
ASO-060	21	UGAGCAUCCAGACAUCUCCAG
ASO-061	21	CUGAGCAUCCAGACAUCUCCA
ASO-062	21	UCUGAGCAUCCAGACAUCUCC
ASO-063	21	CUCUGAGCAUCCAGACAUCUC
ASO-064	21	GCUCUGAGCAUCCAGACAUCU
ASO-065	21	CGCUCUGAGCAUCCAGACAUC
ASO-066	19	CAUCCAGACAUCUCCAGAC
ASO-067	19	AUCCAGACAUCUCCAGACC
ASO-004-01	23	CAGACATCTCCAGACCATCTCTC
ASO-004-02	21	AGACATCTCCAGACCATCTCT
ASO-004-03	19	GACATCTCCAGACCATCTC
ASO-004-04	17	ACATCTCCAGACCATCT
ASO-005-01	23	AGCATCCAGACATCTCCAGACCA
ASO-005-02	21	GCATCCAGACATCTCCAGACC
ASO-005-03	19	CATCCAGACATCTCCAGAC
ASO-005-04	17	ATCCAGACATCTCCAGA

Supplementary Figure 2: List of ASO sequences examined in the micro-tiling and optimization of ASO length phase. All ASO sequences initially were synthesized using 2'-O-Methyl base chemistry and phosphorothioate backbone.

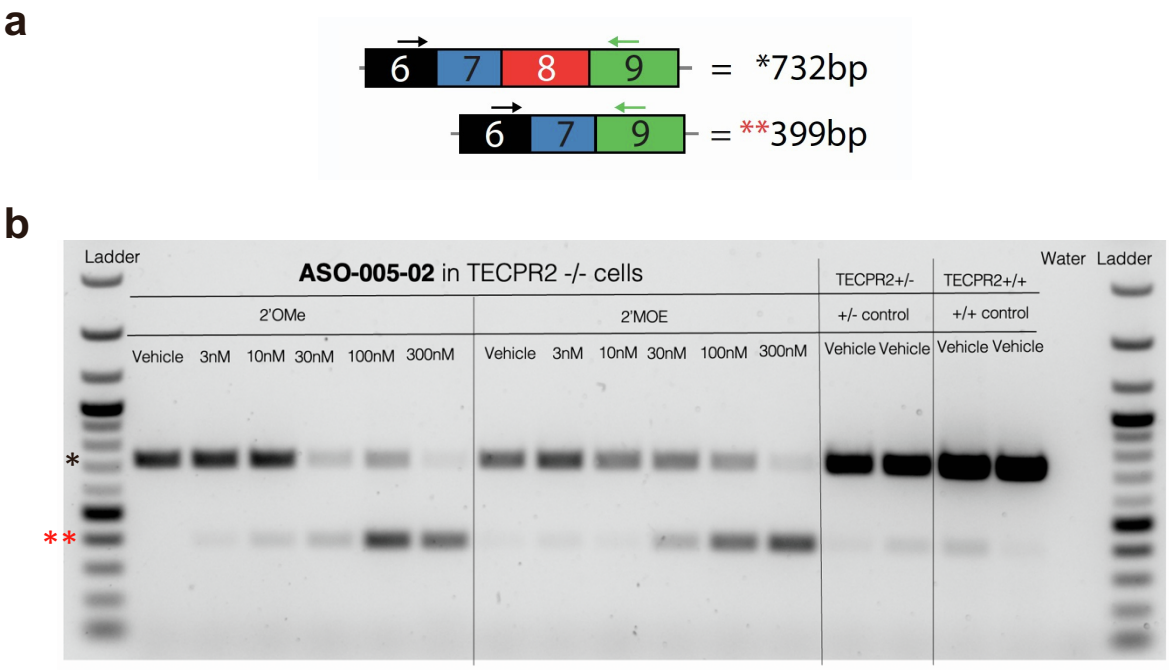

Supplementary Figure 3: Comparison of *TECPR2* Exon 8 skipping activity in TECPR2-/- patient-derived fibroblasts induced by ASO-005-02 sequence synthesized with 2'-O-Methyl (2'OMe) versus 2'-MOE RNA base chemistry. a, Diagram of RT-PCR assay and PCR amplicons to be obtained when *TECPR2* exon 8 is skipped in human fibroblast. **b**, DNA gel inverted image showing PCR results for fibroblast cells derived from *TECPR2-/-* patient treated for 5 days with ASO-005-02 sequence synthesized using two different types of ASO RNA base chemistry (2'-O-methyl (2'OMe) and 2'MOE) and 5 different concentrations (3 nM to 300 nM). Clear enrichment of lower PCR product (~399bp, highlighted by **) can be detected in fibroblast samples treated with either ASO chemistry at 30 nM to 300 nM compared to negative control conditions (vehicle).

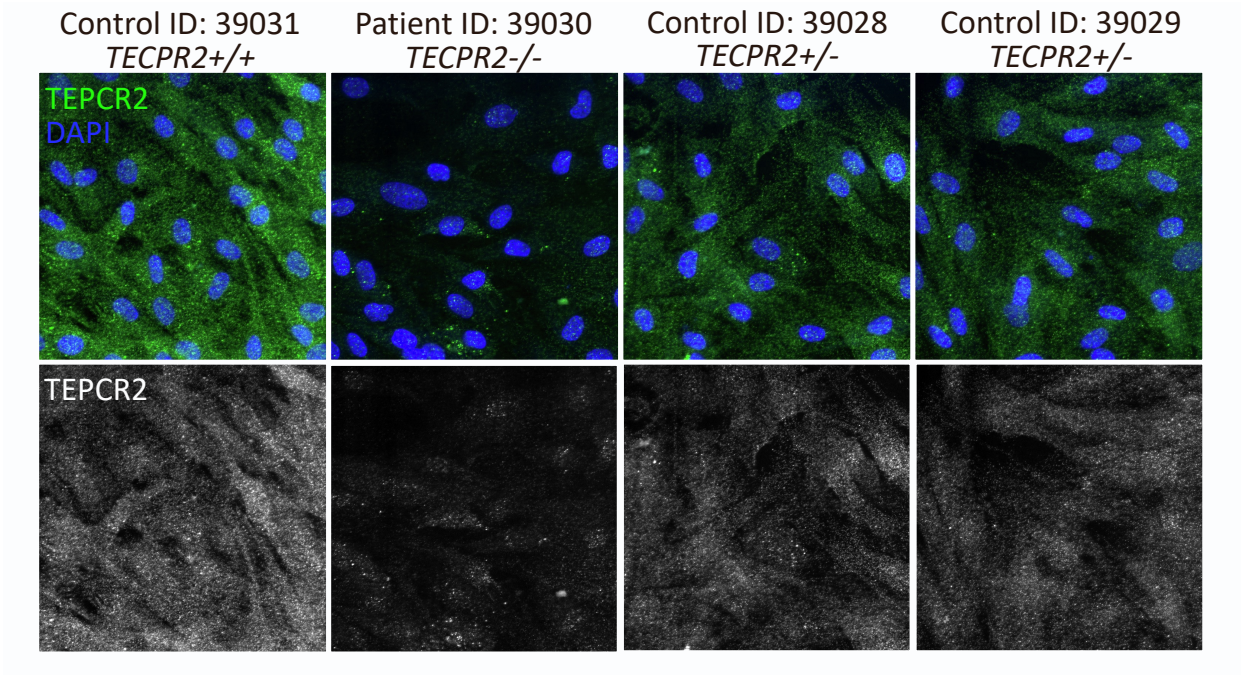

Supplementary Figure 4: Immunofluorescence staining for TECPR2 protein in fibroblast cell lines derived from SPG49 patient and healthy family members. Fibroblast cell lines were generated from skin punch biopsies obtained from the *TECPR2-/-* patient (Cell Line ID: 39030), from a *TECPR2+/+* family member (39031), and from two *TECPR2+/-* family members heterozygous for the *TECPR2* mutation (39028 and 39029). Cultured fibroblasts were analyzed by immunofluorescence staining for TECPR2 protein using a rabbit polyclonal antibody raised against human TECPR2 as the primary antibody. The top row shows the immunofluorescence signal for TECPR2 (green) and nuclear DAPI staining (blue). The bottom row shows the immunofluorescence signal for TECPR2 only. The first column shows immunocytochemistry analysis of homozygous wild type *TECPR2+/+*. The second column shows analysis of *TECPR2-/-* SPG49 patient fibroblasts. The third and fourth columns show analysis of heterozygous *TECPR2+/-* fibroblast cell lines from two of the patient's family members that are heterozygous for the patient's *TECPR2* mutation. As seen in column two, there is a substantial loss of TECPR2 immunoreactivity signal in fibroblast cells derived from the SPG49 patient, compared to either *TECPR2+/+* cells or *TECPR2+/-* cells.

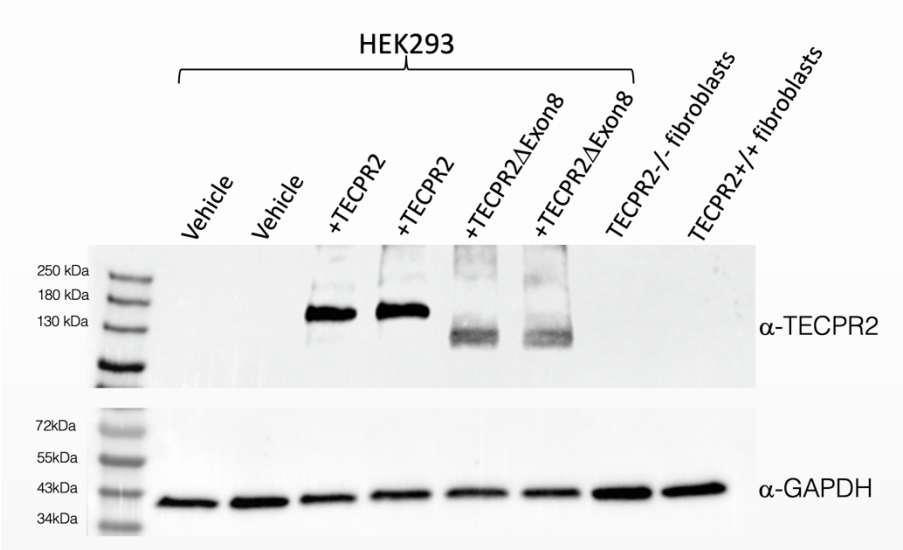

Supplementary Figure 5: TECPR2 antibody can detect overexpression of TECPR2 full length protein and TECPR2ΔExon8 protein variants, but not endogenous levels of TECPR2 protein in HEK293 cells and human fibroblasts. To determine if the TECPR2 polyclonal antibody used for immunocytochemistry assays could detect TECPR2 full length and TECPR2ΔExon8 protein levels, DNA expression constructs containing either cDNA variant were transfected into HEK293 cells using Lipofectamine. Protein lysates were collected after 72 hours from each of 2 replicate wells per condition and separated by SDS-PAGE after loading 30 µg of total HEK293 protein lysate. Immunoblotting assays with the TECPR2 polyclonal antibody detected a protein band at ~180KDa, corresponding to the predicted size of full length TECPR2 in samples treated with the TECPR2 cDNA expression construct, and a lower molecular weight species corresponding to a shorter variant of TECPR2 lacking 111 amino acids from *TECPR2* Exon 8 in samples transfected with the TECPR2ΔExon8 cDNA. Endogenous TECPR2 protein signal was not detected in either HEK293 cell extracts treated with vehicle or in 25 µg protein lysates obtained from TECPR2+/+ and TECPR2-/- fibroblasts. Immunoblotting against housekeeping protein GAPDH was used to demonstrate protein loading. These results suggest that using immunoblotting to measure endogenous levels of TECPR2 and TECPR2ΔExon8 protein variant induced by Exon 8 skipping in the human fibroblast assay is not feasible with this immunoreagent.

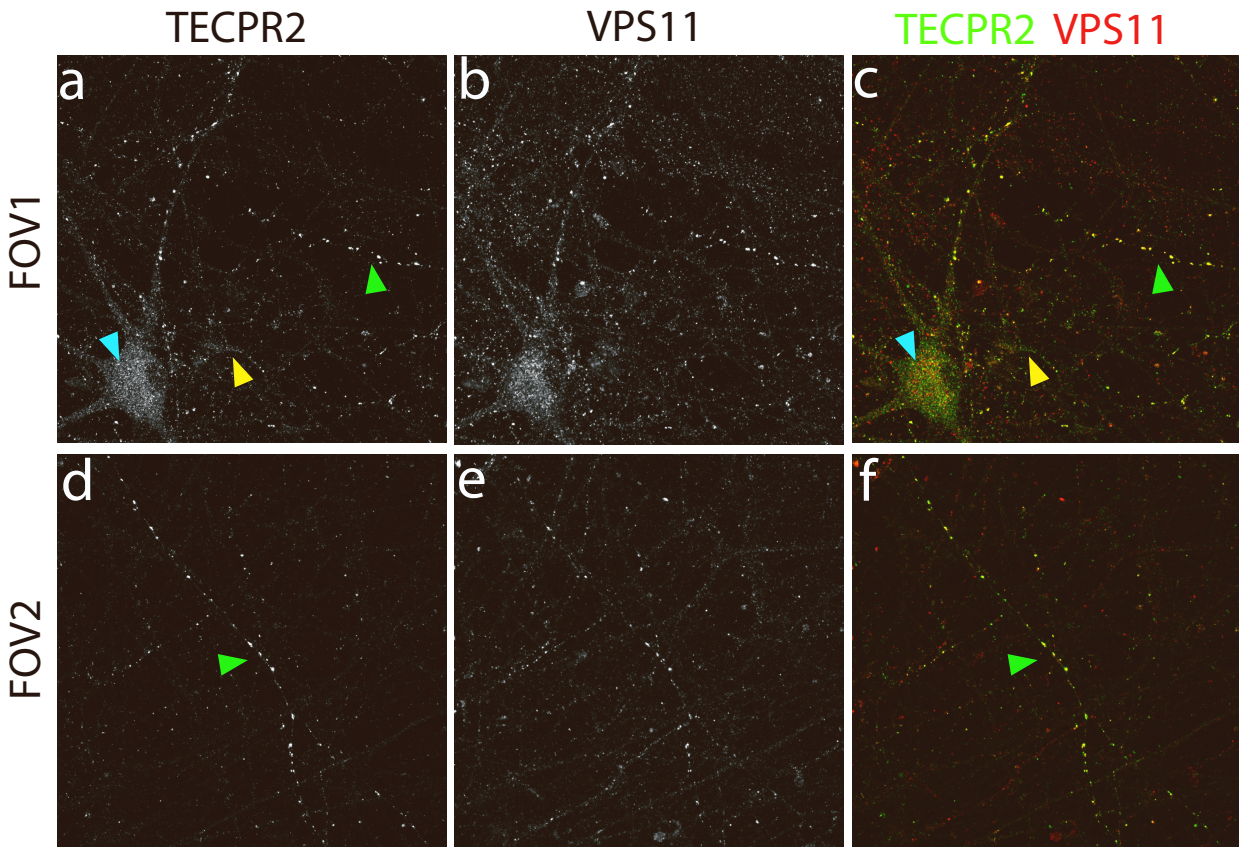

Supplementary Figure 6: Immunocytochemistry analyses showing co-localization of TECPR2 protein with vesicle-mediated trafficking protein VPS11 (Vacuolar Protein Sorting-associated protein 11 homolog) in *TECPR2*+/+ iPSC-derived neurons (DIV45). Two different fields of view (FOV1 and FOV2) are presented, with panels **a** and **d** showing TECPR2 immunoreactivity signal. In these panels, cyan arrowhead shows TECPR2 puncta localization in soma, yellow arrowhead shows small discrete TECPR2 positive puncta in neurites, and green arrowheads show rare large TECPR2 puncta in neuronal processes. Panels **b** and **e** show VPS11 immunoreactivity signal for the same FOV1 and FOV2, respectively. Significant overlap of TECPR2 (in green) and VPS11 (in red) immunoreactivity signal can be detected in the merged panels **c** and **f**, where the three arrowheads indicate the three different types of TECPR2/VPS11 positive puncta which can be detected by a yellow signal.

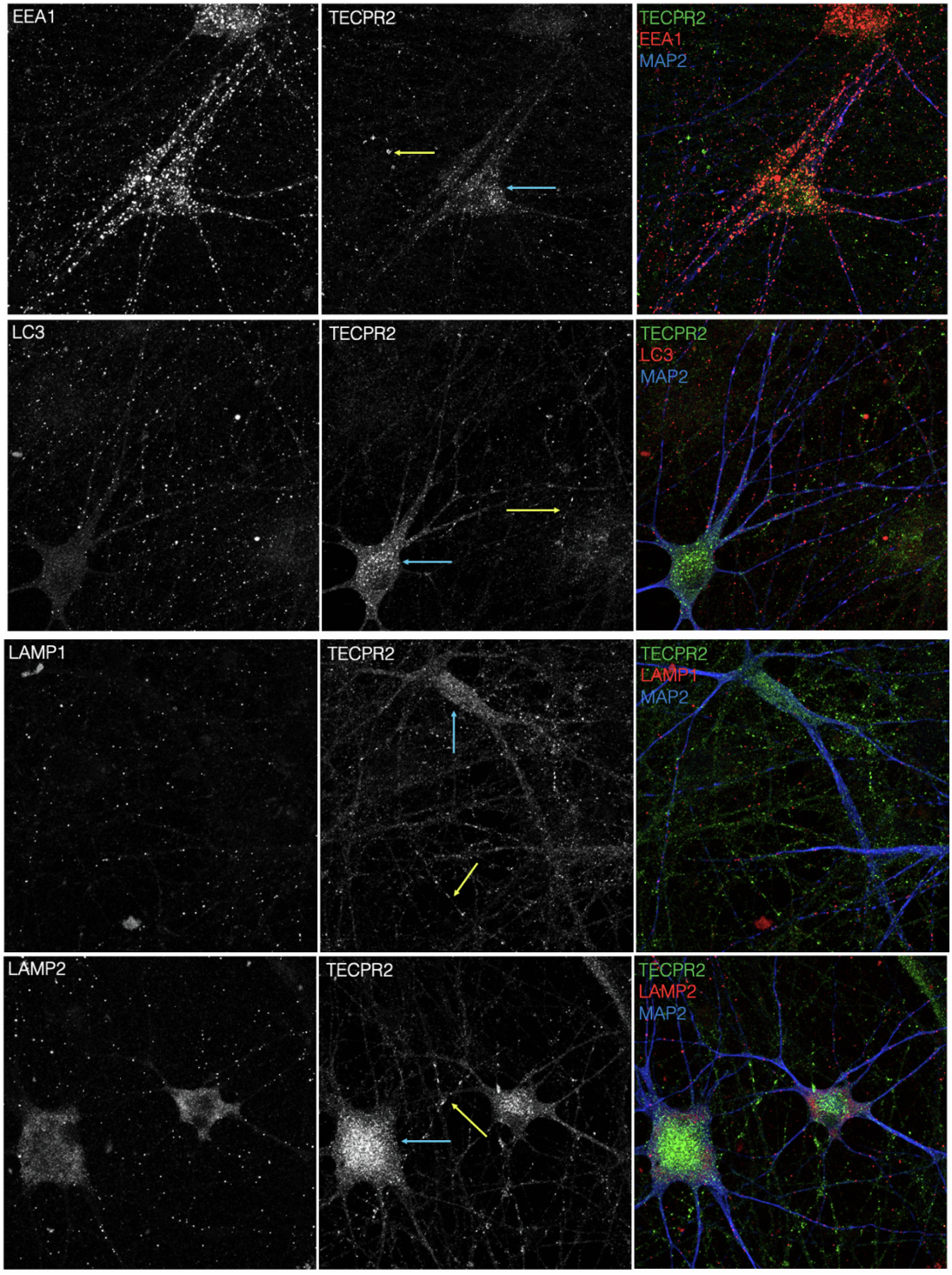

Supplementary Figure 7: Immunocytochemistry analyses showing lack of co-localization of TECPR2 protein puncta with additional autophagy and lysosomal markers in human iPSC-derived neurons. Given the reported association of TECPR2 with autophagy and ER export[1,4], we assessed co-localization of TECPR2 with EEA1 (Early Endosome Antigen 1), LAMP1 (Lysosomal-Associated Membrane Protein 1), LAMP2, and the autophagy cargo marker LC3 (Microtubule-Associated Protein 1A/1B-Light Chain 3) in *TECPR2*+/+ iPSC-derived NGN2 neurons (DIV45). We did not detect significant co-localization of TECPR2 with any of these markers, including in the large TECPR2-positive puncta as indicated by arrows in the panels above, suggesting that in these neurons, TECPR2 protein has a subcellular localization that is distinct from canonical endosomal, lysosomal and autophagosomal compartments.

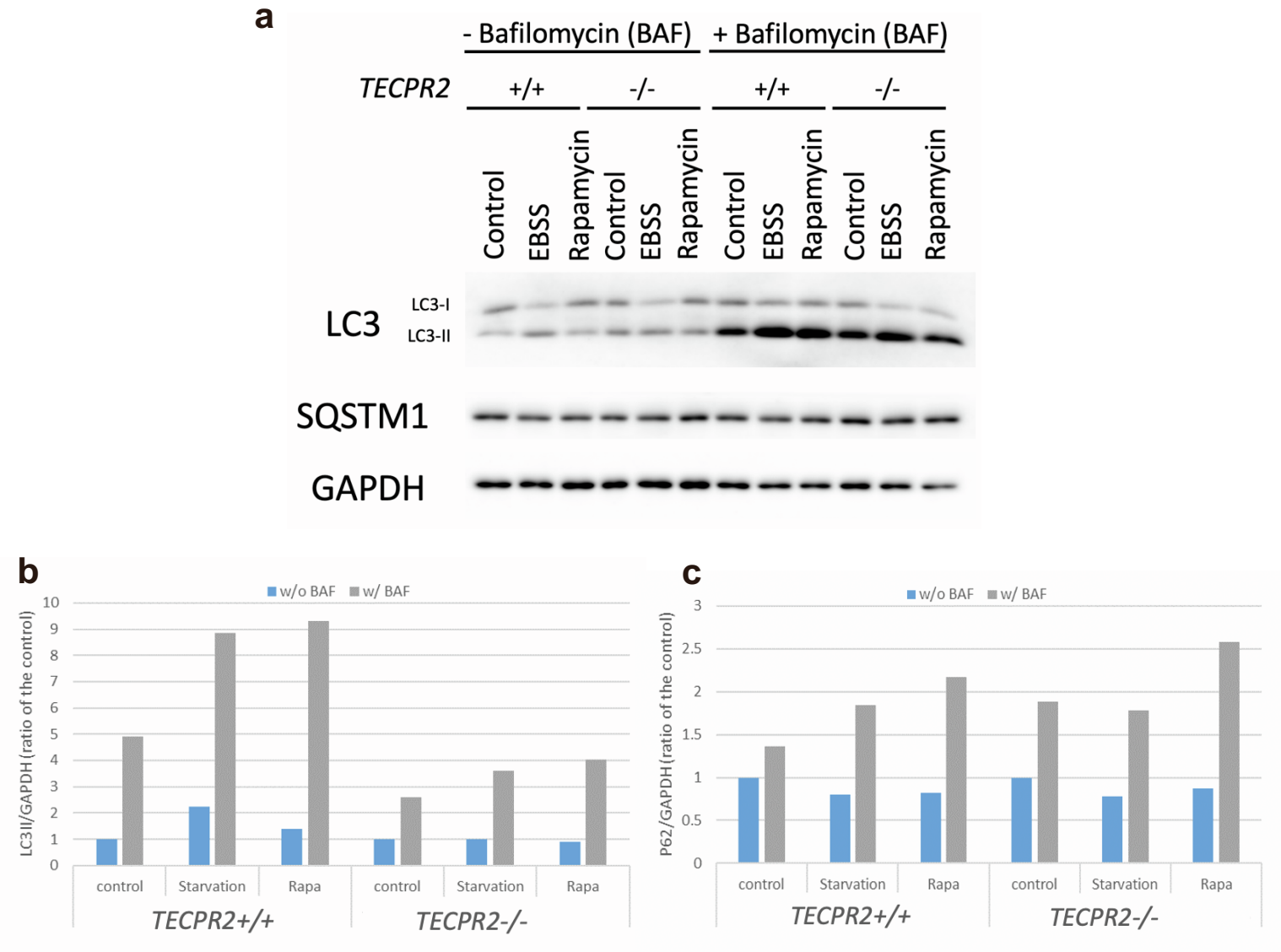

Supplementary Figure 8: Preliminary autophagy assays with *TECPR2-/-* patient and healthy *TECPR2+/+* control fibroblasts did not reveal a clear impact of loss of TECPR2 on basal autophagy or the response to autophagy inducers. a, MAP1LC3B (LC3) lipidation and SQSTM1 (p62) protein levels in human *TECPR2+/+* and *TECPR2-/-* fibroblasts cultured in complete medium (control), starvation inducing medium (EBSS), or complete medium supplemented with 5 uM Rapamycin (RAPA), with or without 25 nM Bafilomycin A1 (BAF) treatment for 6 hours. Levels for the housekeeping protein GAPDH were used as a loading control. **b**, Lipidated LC3 (LC3-II) and **c**, SQSTM1 (p62) protein levels normalized to GAPDH were compared to control condition for each *TECPR2* genotype. While *TECPR2-/-* cells appear to exhibit a mild defect in LC3-II lipidation in response to conventional autophagy activators (starvation and Rapamycin administration) as compared to *TECPR2-/-* cells (which can be maximally appreciated in the presence of the lysosomal inhibitor bafilomycin A1), the lysosome-dependent degradation of autophagy substrates like p62 is not affected by loss of TECPR2. Given that these fibroblast cell lines are not syngeneic, additional studies using multiple cell lines and other cell types such as neurons are warranted.

a

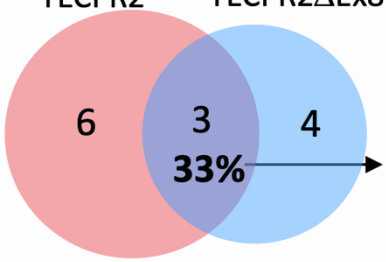

TECPR2 and TECPR2ΔEx8 interactions

Protein	TECPR2 logOdds	TECPR2ΔEx8 logOdds
FLNA	79.1	65.16
MCM3	45.24	56.81
PRKDC	49.62	72.64

	Protein	TECPR2 logOdds	TECPR2ΔEx8 logOdds
TECPR2 interactions	EPPK1	40.2	25.67
	USP7	71.75	38.5
	VPS16	42.89	
	VPS18	55.93	
	VPS33A	58.81	
	VPS41	51.59	
TECPR2ΔEx8 interactions	DNAJA1	26.68	45.76
	MCM5	31.13	44.31
	MCM7	29.13	43.79
	USP9X	39.94	42.85

b

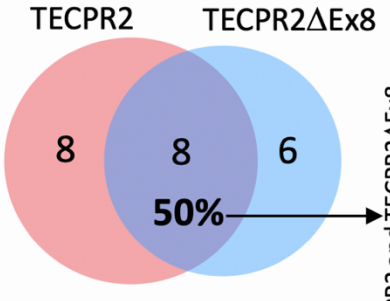

TECPR2 and TECPR2ΔEx8 interactions

Protein	TECPR2 logOdds	TECPR2ΔEx8 logOdds
FLNA	79.1	65.16
HSPH1	32.6	32.6
MCM3	45.24	56.81
MCM5	31.13	44.31
PFKP	37.04	35.57
PRKDC	49.62	72.64
USP7	71.75	38.5
USP9X	39.94	42.85

	Protein	TECPR2 logOdds	TECPR2ΔEx8 logOdds
TECPR2 interactions	VPS16	42.89	
	VPS18	55.93	
	VPS33A	58.81	
	VPS41	51.59	
	EPPK1	40.2	25.67
	IRS2	34.08	25.18
	NUP155	35.06	23.19
	PARD3	32.64	26.69
TECPR2ΔEx8 interactions	ACLY	25.18	34.08
	BLOC1S5	26.71	34.1
	DNAJA1	26.68	45.76
	DNAJA2	20.69	32.62
	MCM7	29.13	43.79
	SERPINH1	17.63	32.62

c

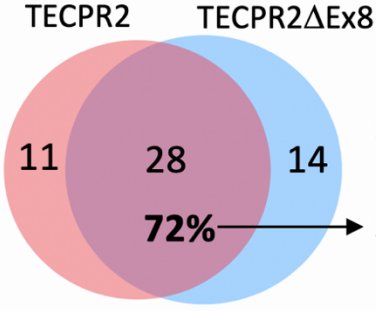

TECPR2 and TECPR2ΔEx8 interactions

Protein	TECPR2 logOdds	TECPR2ΔEx8 logOdds
ACLY	25.18	34.08
ACOT9	20.69	29.67
BLOC1S5	26.71	34.1
CCT2	23.5	22.31
CYTIP	26.71	26.69
DNAJA1	26.68	45.76
DNAJA2	20.69	32.62
DNAJC7	23.71	25.2
DOCK6	20.69	20.68
DOCK7	20.69	20.68
DTNBP1	23.71	29.67
EPPK1	40.2	25.67
FLNA	79.1	65.16
HSPA4L	23.68	20.66
HSPH1	32.6	32.6
IRS2	34.08	25.18
MCM3	45.24	56.81
MCM5	31.13	44.31
MCM7	29.13	43.79
MTHFD1L	28.2	20.68
NUP155	35.06	23.19
PARD3	32.64	26.69
PFKP	37.04	35.57
PRKDC	49.62	72.64
SNX27	26.71	26.69
UBA1	28.16	29.65
USP7	71.75	38.5
USP9X	39.94	42.85

	Protein	TECPR2 logOdds	TECPR2ΔEx8 logOdds
TECPR2 interactions	BLOC1S3	25.21	19.16
	CSNK2A1	28.2	
	CSNK2A2	26.71	
	CSNK2A3	28.2	
	DYNC1H1	25.21	19.16
	KPNA1	23.21	
	PLK1	22.21	11.33
	VPS16	42.89	
	VPS18	55.93	
	VPS33A	58.81	
	VPS41	51.59	
TECPR2ΔEx8 interactions	CARNS1	19.17	22.19
	CCT3	15.3	24.44
	CCT5	13.63	21.14
	GMPS	14.53	20.68
	HUWE1	19.17	22.19
	NUDC	17.63	20.68
	PGAM5	18.84	24.28
	PLS1	19.14	23.68
	PLS3	19.14	23.68
	PSMD2	9.7	25.2
	RUVBL1	12.91	22.17
	SERPINH1	17.63	32.62
	SLC25A1	14.53	20.68
	USP11	17.63	25.2

Supplementary Figure 9: Preliminary interactome studies in HEK293 cells with stable expression of HA-tagged TECPR2 and TECPR2ΔExon8 protein variants suggest that a significant percentage (33%-72%) of protein interactors with full-length TECPR2 also interact with TECPR2ΔEx8. To identify potential TECPR2 protein interactors, and to compare interactors of full-length TECPR2 and TECPR2ΔEx8 in cells, pull-down experiments using stable expression of HA-tagged TECPR2 (full-length) and HA-tagged TECPR2ΔEx8 in *TECPR2-/-* HEK293 cells were performed, followed by identification of proteins that were pulled down using mass spectrometry-based proteomics. A stringent Bayesian False Discovery Rate (BFDR) of 0.01 statistical threshold was used to define interactors. Log of Odds ratios (LOR) of 40, 30 and 20 were applied to the identified interactors to define likely significant interaction candidates over a range of statistical thresholds (see methods for additional experimental details). **a-c**, Venn diagrams highlighting the percentage of TECPR2 protein interactions that are retained by the TECPR2ΔEx8 variant, along with tables listing the candidate protein interactors defined using different Log of Odds ratios (LOR) statistical thresholds: (**a**) LOR 40, with 3 out of 9 (33%) defined candidate interactions for TECPR2 retained by TECPR2ΔEx8, (**b**) LOR 30, with 8 out 16 (50%) defined candidate interactions for TECPR2 retained by TECPR2ΔEx8, (**c**) LOR 20, with 28 out 39 (72%) defined candidate interactions TECPR2 retained by TECPR2ΔEx8. From these analyses, there is evidence that a significant percent of interactors with full-length TECPR2 also interact with TECPR2ΔEx8. The estimated percentage of retained interactions ranges from 33% - 72%, depending on the statistical thresholds used for the analysis. It is not straightforward to describe potential TECPR2 functions that may be retained by TECPR2ΔEx8 or to estimate how this may relate to therapeutic efficacy of ASO-005-02 from examining the set of retained protein interactors. It is also of note that there are 8 proteins (VPS41, VPS33A, VPS16, VPS18, CSKN2A1, CSKN2A2, CSKN2A3 and KPNA1) that were identified as interactors of TECPR2, yet not found to interact with TECPR2ΔEx8. TECPR2 functions associated with interactions with these proteins, although unknown, may not be restored by TECPR2ΔEx8. There was not strong evidence that any proteins interact exclusively with the TECPR2ΔEx8 form. However, a few proteins seem to have a stronger interaction with TECPR2ΔEx8 than the full-length form: DNAJA1, DNAJA2, MCM3, MCM5 and MCM7. One of the challenges of this approach is that it is not possible to predict which TECPR2 interactome mediated functions may be retained by TECPR2ΔEx8 or to estimate how this may relate to therapeutic efficacy of ASO-005-02. This is in large part due to the state of limited knowledge regarding the function of TECPR2 and the functions of its interacting partners.

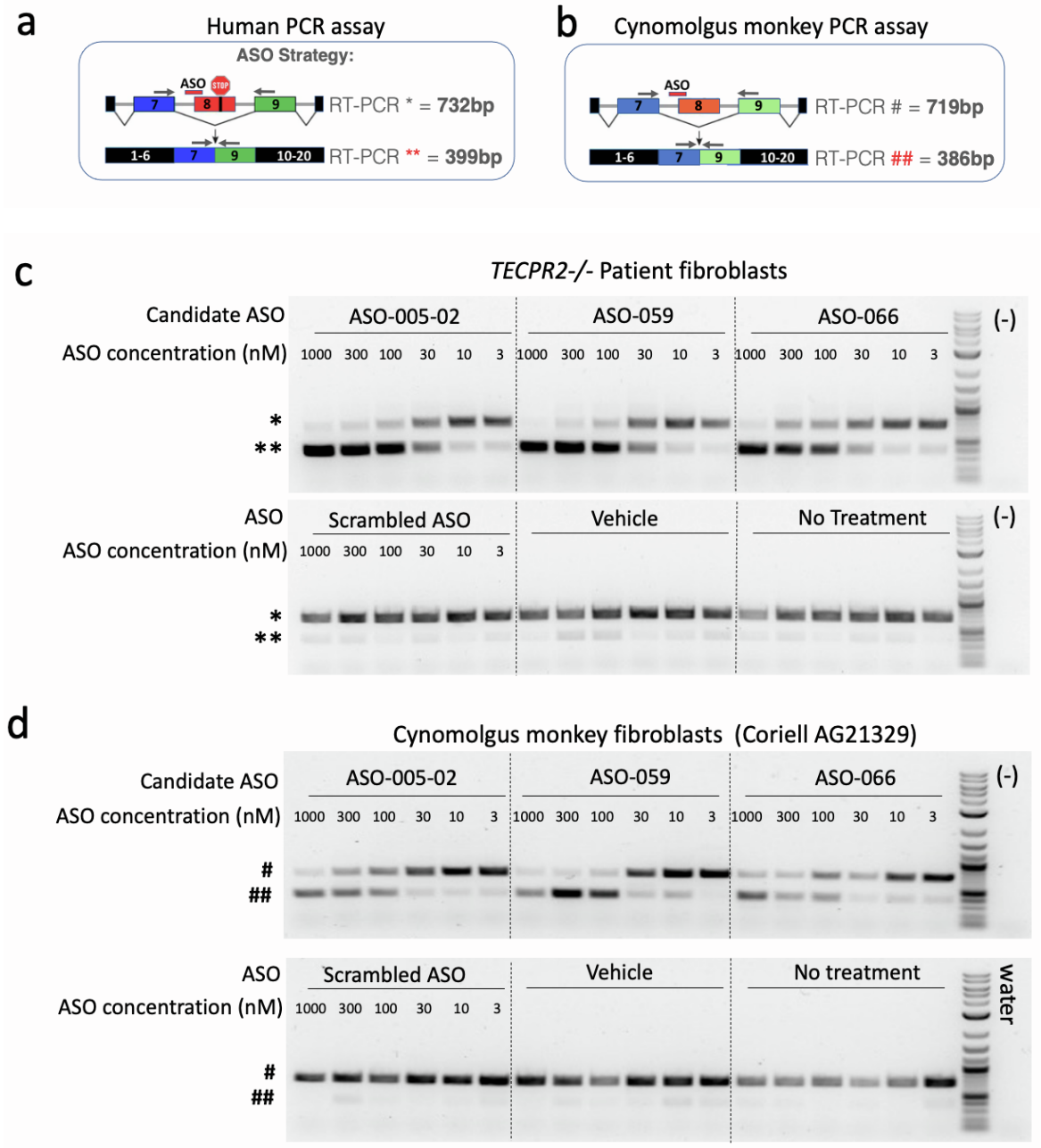

Supplementary Figure 10: Assessment of top 3 ASO lead candidates in cultured cynomolgus monkey fibroblasts prior to *in vivo* tolerability studies. a,b Diagram of RT-PCR assay and PCR amplicons to be obtained when *TECPR2* exon 8 is skipped in patient-derived cells (a) or in cultured cynomolgus monkey fibroblasts (b). **c**, DNA gel inverted images showing PCR results for patient fibroblasts treated with ASO leads ASO-005-02, ASO-059 and ASO-066 at different concentrations (1000 nM to 3 nM). Enrichment of lower PCR product (~399bp, highlighted by **) can be detected in samples treated with 30 nM to 1000 nM of each of the 3 ASOs compared to negative control conditions (scrambled non-targeting ASO sequence, vehicle, and No Treatment). **d**, DNA gel inverted images showing PCR results for cultured cynomolgus fibroblasts treated with ASO leads ASO-005-02, ASO-059 and ASO-066 at different concentrations (1000 nM to 3 nM). Enrichment of lower PCR product (~386bp, highlighted by ##) can be detected in samples treated with 100 nM to 1000 nM of each of the 3 ASOs compared to negative control conditions (scrambled non-targeting ASO sequence, vehicle, and No Treatment).

The objective of this NHP study was to determine the tolerability and lead selection of 3 candidate antisense oligonucleotides (ASOs): ASO-059 (Lot ID: QS0321489-05), ASO-005-02 (QS0321490-05), ASO-066 (QS0321491-05) when given by a single intrathecal injection to monkeys. In addition, the biodistribution characteristics of each candidate were determined. The study design was as follows:

Group No.	Test Material	Dose Level (mg/dose)	Dose Volume (mL/dose)	Dose Concentration (mg/mL)	Animal Numbers	
					Main Study	
					Males	Females
1	Reference Item (Elliotts B)	0	1	0	1001	-
2	QS0321489-05 (ASO-059)	20	1	20	2001	2501
3	QS0321490-05 (ASO-005-02)	20	1	20	3001	3501
4	QS0321491-05 (ASO-066)	20	1	20	4001	4501

QS0321489-05, QS0321490-05, and QS0321491-05, formulated in Elliotts B solution, was administered by direct intrathecal puncture at the lumbar level on Day 1. The following parameters and end points were evaluated in this study: mortality, clinical observations, body weights, neurological examinations, cerebrospinal fluid (CSF) and tissue bioanalysis (samples collected at necropsy), tissue mRNA splicing analysis, gross necropsy findings, and histopathological examinations.

There was no mortality during the study.

There were no QS0321489-05-, QS0321490-05-, and QS0321491-05-related effects on body weights and pathology findings (macroscopic and microscopic).

Administration of QS0321489-05, QS0321490-05, and QS0321491-05 resulted in similar clinical signs, consisting of tremors, decreased activity, partly closed eyes, hunched posture, and/or emesis. These clinical observations were generally more prominent in females; however due to the small population size in the study, this should be interpreted with caution. Clinical signs were noted as early as 4 hours post-dose on Day 1 and had generally resolved by the following day. These clinical signs were consistent with findings in the animals' general attitude and motor function noted at the 5-hour post-dose neurological examination. Additionally, decreased muscle tone and/or flexor reflex were observed in one or both hindlimbs in Animal Nos. 2501, 3001, 3501, and 4501. Neurological changes were more prominent in Animal No. 3501 administered QS0321490-05 at 20 mg, which also demonstrated a lack of visual and tactile placing reactions of both hindlimbs. At 24 hours post-dose, decreased visual placing reactions and/or flexor reflexes (hindlimbs and forelimbs) were still evident but did not correlate with any abnormal clinical observations. There were no abnormal changes noted on Day 15.

Bioanalytical results for samples collected at necropsy showed that concentration of QS0321489-05 and QS0321491-05 in CSF was detected in 1 out of 2 animals (female only) and concentration of QS0321490-05 was detected in both animals. Concentration of QS0321489-05, QS0321490-05, or QS0321491-05 was detected in the tissue samples from both animals in each group. There was moderate inter-animal variability observed for all 3 ASOs and a trend towards QS0321490-05 generally yielding higher concentrations in many tissue samples.

Tissue mRNA splicing analysis demonstrated that there was clear evidence of *TECPR2* exon8-skipping activity in CNS tissue samples. A clear relationship between the degree of exon8 skipping and ASO concentration was observed among a subset of CNS tissues analyzed from the two animals treated with QS0321490-05.

In conclusion, administration of QS0321489-05, QS0321490-05, or QS0321491-05 by a single intrathecal injection resulted in transient clinical signs and neurological changes, which were similar in nature for all 3 ASOs. Concentrations of QS0321489-05, QS0321490-05, or QS0321491-05 were detected in all tissue samples and generally in 1 of 2 CSF samples. Tissue mRNA splicing analysis revealed that QS0321490-05 demonstrated the best exon8-skipping activity among the three ASOs; and therefore, was chosen as the lead candidate for the subsequent study.

Supplementary Figure 11: Summary report for non-human primate tolerability study.

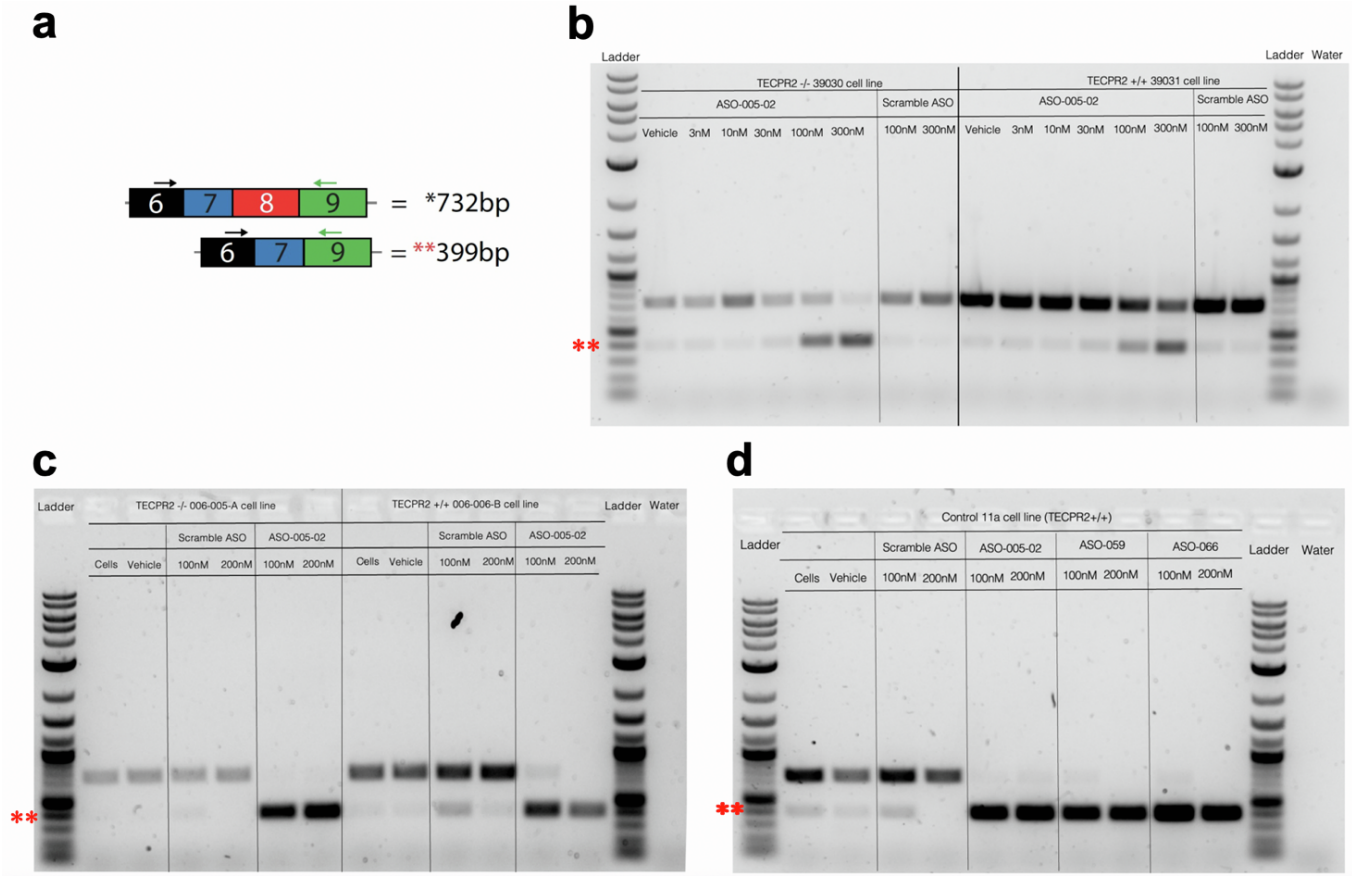

Supplementary Figure 12: Top ASO lead candidate (ASO-005-02) induces TECPR2 Exon 8 skipping activity in *TECPR2*+/+ control cellular reagents (dermal fibroblasts and human iPS cell-derived neurons). a, Diagram of RT-PCR assay and PCR amplicons to be obtained when *TECPR2* exon 8 is skipped in human fibroblast and iPS cell-derived neurons. **b**, DNA gel inverted image showing PCR results for fibroblast cells derived from *TECPR2-/-* patient (39030 cell line) and *TECPR2*+/+ healthy control (39031 cell line) treated for 5 days with ASO lead candidate ASO-005-02, at different concentrations (3 nM to 300 nM). Clear enrichment of lower PCR product (~399bp, highlighted by **) can be detected in samples treated with 100 nM to 300 nM compared to negative control conditions (scrambled non-targeting ASO sequence and vehicle). **c**, DNA gel inverted image showing PCR results for cultured human iPS cell-derived neurons derived from *TECPR2-/-* patient (006-005-A cell line) and *TECPR2*+/+ healthy control (006-006B cell line) treated for 7 days with ASO lead candidate ASO-005-02, at two different concentrations (100 nM and 200 nM). Clear enrichment of lower PCR product (~399bp, highlighted by **) can be detected at both concentrations compared to negative control conditions (scrambled non-targeting ASO sequence, vehicle and untreated cells). For this experiment, ASO was delivered into the cultured neurons using optimized transfection conditions with a polypeptide delivery reagent (vehicle). **d**, DNA gel inverted image showing PCR results for cultured human neurons derived from a *TECPR2*+/+ iPS cell line (Control 11a cell line) obtained from a different healthy donor. Cultured neurons were treated for 7 days with the top ASO lead candidate (ASO-005-02) and two back-up candidates (ASO-059 and ASO-066) at two different concentrations (100 nM and 200 nM). Clear enrichment of lower PCR product (~399bp, highlighted by **) can be detected at both concentrations compared to negative control conditions (scrambled non-targeting ASO sequence, vehicle and untreated cells). For this experiment, ASO leads were delivered into the cultured neurons using optimized transfection conditions with a polypeptide delivery reagent (vehicle). "Water" for all PCR experiments indicates a negative control sample in which cDNA was not added to the PCR assay.

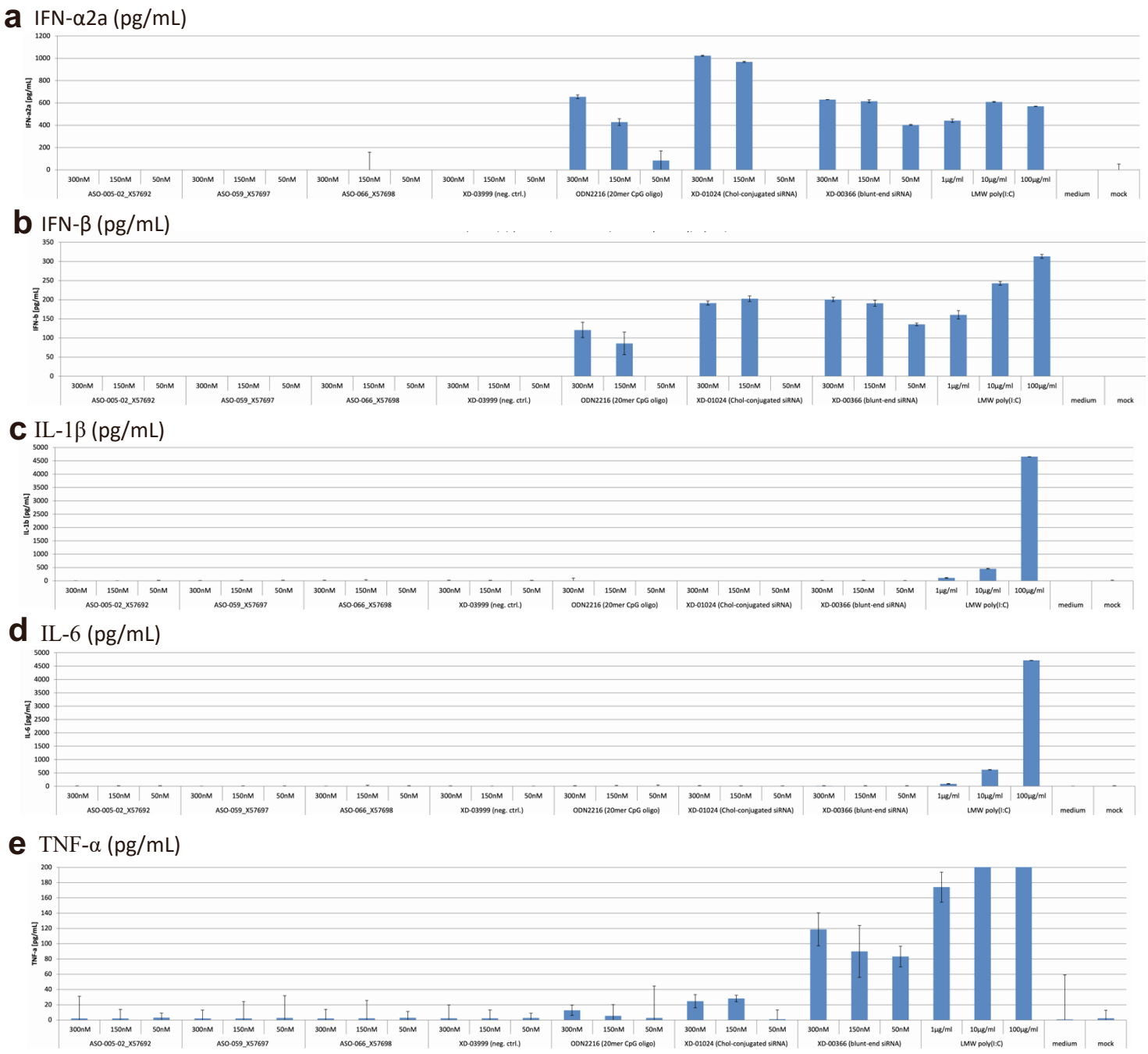

Supplementary Figure 13: ASO lead candidate (ASO-005-02) and two back-up candidates (ASO-059 and ASO-066) are inactive in human PBMC cytokine release assays. ASO molecules were delivered at 3 different concentrations (50 nM, 150 nM, 300 nM) into human peripheral blood mononuclear cells via lipid-based transfection (Lipofectamine 2000) and the levels for 5 different cytokines: (a) IFN-α2a, (b) IFN-β, (c) IL-1β, (d) IL-6, (e) TNF-α were measured and analyzed using MSD platform 24 hrs after transfection. None of the 3 ASO molecules tested induced upregulation in cytokine release. Multiple positive controls (inflammatory stimuli) were used, including a TLR7/8 agonist (XD-01024, a cholesterol-conjugated ApoB siRNA), a TLR9 agonist (ODN2216, a 20mer CpG oligo containing unmethylated CpG), a TLR7/8 agonist (XD-00366, a 25mer double-stranded, unmodified, blunt-ended LacZ RNA duplex), and a TLR3, RIG-I/MDA5 and PKR agonist (LMW poly(I:C): low molecular weight polyinosinic-polycytidylic acid). A chemically modified siRNA (XD-03999) against FVII was used as negative control.